Addition of a carboxy terminal tail to the normally tailless gonadotropin-releasing hormone receptor impairs fertility in female mice

Chirine Toufaily[1], Jérôme Fortin[1], Carlos A. I. Alonso[1], Evelyn Lapointe[2], Xiang Zhou[1], Yorgui Santiago-Andres[3], Yeu-Farn Lin[1], Yimming Cui[1], Ying Wang[1], Dominic Devost[1], Ferdinand Roelfsema[4], Frederik Steyn[5,6], Aylin C. Hanyaloglu[7], Terence E. Hébert[1], Tatiana Fiordelisio[3], Derek Boerboom[2], and Daniel J. Bernard[1]*

[1]Department of Pharmacology and Therapeutics, McGill University, Montreal, Québec, Canada.
[2]Département de biomédecine vétérinaire, Université de Montréal, Saint-Hyacinthe, Québec, Canada.
[3]Departamento de Ecología y Recursos Naturales, Biología, Facultad de Ciencias, Universidad Nacional Autónoma de México, Ciudad Universitaria, Ciudad de México, México
[4]Department of Internal Medicine, Section Endocrinology and Metabolic Diseases, Leiden University Medical Center, Leiden, The Netherlands.
[5]School of Biomedical Sciences, Faculty of Medicine, The University of Queensland, Brisbane, Australia.
[6]Department of Neurology, Royal Brisbane & Women's Hospital, Queensland, Brisbane, Australia.
[7]Institute of Reproductive and Developmental Biology, Department of Metabolism, Digestion and Reproduction, Imperial College London, London, United Kingdom.

*Address correspondence: Daniel J. Bernard, Ph.D., Department of Pharmacology and Therapeutics, McGill University, 3655 Promenade Sir William Osler, Montreal, Québec, Canada, H3G 1Y6. daniel.bernard@mcgill.ca

Funding: This work was supported by the Canadian Institutes of Health Research operating grants MOP-123447 and PJT-252739 to DJB; the Mexican National Counsel of Science and Technology operating grant CONACYT 273513 and the National University of Mexico operating grant PAPITT IN227416 to TF. TEH holds the Canadian Pacific Chair in Biotechnology.

ABSTRACT

Gonadotropin-releasing hormone (GnRH) is the primary neuropeptide controlling reproduction in vertebrates. GnRH stimulates follicle-stimulating hormone (FSH) and luteinizing hormone (LH) synthesis via a G protein-coupled receptor, GnRHR, in the pituitary gland. In mammals, GnRHR lacks a C-terminal cytosolic tail (Ctail) and does not exhibit homologous desensitization. This might be an evolutionary adaptation that enables LH surge generation and ovulation. To test this idea, we fused the chicken GnRHR Ctail to the endogenous murine GnRHR in a transgenic model. The LH surge was blunted, but not blocked in these mice. In contrast, they showed reductions in FSH production, ovarian follicle development, and fertility. Addition of the Ctail altered the nature of agonist-induced calcium signaling required for normal FSH production. The loss of the GnRHR Ctail during mammalian evolution is unlikely to have conferred a selective advantage by enabling the LH surge. The adaptive significance of this specialization remains to be determined.

INTRODUCTION

The propagation and survival of all species depends on reproduction. In vertebrates, the process is controlled by hormones in the hypothalamic-pituitary-gonadal axis. Arguably, the hypothalamic decapeptide gonadotropin-releasing hormone (GnRH) is the most important brain hormone regulating reproduction (1-4). Disruption of GnRH synthesis, secretion, or action can delay or prevent puberty or cause infertility. GnRH acts via its receptor, GnRHR, in pituitary gonadotrope cells. GnRHR agonists and antagonists are used clinically in assisted reproductive technologies and to treat hormone-dependent diseases (2, 5-7).

GnRH is released in pulses from neuron terminals in the median eminence into the pituitary portal vasculature. The hormone binds GnRHR on the plasma membrane of gonadotropes, stimulating the synthesis and secretion of the gonadotropins, luteinizing hormone (LH) and follicle-stimulating hormone (FSH) (8-12). LH and FSH are heterodimeric glycoproteins composed of the gonadotropin α subunit (product of the *Cga* gene) non-covalently linked to hormone-specific β-subunits: LHβ (*Lhb*) or FSHβ (*Fshb*), respectively (13-15). GnRH stimulates the expression of all three gonadotropin subunit genes (16-18) as well as its own receptor (*Gnrhr*) (18-21).

LH and FSH regulate gonadal function, most notably steroidogenesis and gamete maturation (22-24). Gonadal sex steroids negatively feedback to the hypothalamus to control their own synthesis by inhibiting GnRH secretion (25-27). In addition, in females, in the late follicular phase of the menstrual cycle in primates or in the afternoon of proestrus in the rodent estrous cycle, high estrogen levels stimulate GnRH secretion through positive feedback, generating a high amplitude, long duration surge of LH, which triggers ovulation (28).

The type 1 GnRHR is a rhodopsin-like G-protein coupled receptor (GPCR) (29). Remarkably, in mammals, GnRHR lacks the intracellular carboxyl-tail (Ctail) that is characteristic of most GPCRs, including GnRHRs in non-mammalian vertebrates like birds, amphibians, and fish (30). The Ctail plays important roles in GPCR function. Agonist binding to many GPCRs leads to receptor internalization and homologous desensitization (31). These processes are often mediated by the phosphorylation of the Ctail by G-protein receptor kinases, recruitment of adaptor proteins such as β-arrestins 1 and 2, and receptor endocytosis via a clathrin-dependent pathway (32, 33). Upon ligand binding, the mammalian GnRHR is not phosphorylated, does not recruit arrestins, and is internalized slowly and with poor efficiency (34-37). Thus, the mammalian

GnRHR is not subject to homologous desensitization in the conventional sense. As a result, the receptor has the potential to continue signaling during times of protracted GnRH secretion, as occurs prior to ovulation. Some have speculated, therefore, that the loss of the Ctail during evolution may have conferred an ability to the mammalian GnRHR to broker long duration, high amplitude LH surges (37, 38), but this was never before addressed directly *in vivo*. It is notable, however, that LH surges are observed in non-mammalian vertebrates with GnRHRs containing Ctails, such as birds (39). Moreover, GnRHRs lacking Ctails have been observed in some non-mammalian vertebrates (40, 41).

To gain greater insight into the potential significance of the loss of the Ctail in the mammalian GnRHR, we generated a knockin mouse model that expresses a chimeric GnRHR in which the chicken GnRHR Ctail was fused in frame to the C-terminus of the murine GnRHR. Importantly, the addition of a chicken Ctail altered, but did not prevent LH surges. Unexpectedly, the data provide novel insight into mechanisms of GnRH-stimulated FSH synthesis.

RESULTS

Generation of knock-in mice expressing a chimeric murine/chicken GnRHR

Using gene targeting in embryonic stem cells, we generated knock-in mice in which the endogenous exon 3 of *Gnrhr* was replaced by a modified exon 3 encoding the C-terminus of murine GnRHR fused in-frame with the intracellular Ctail of the chicken GnRHR (Figure 1-figure supplement 1A-B). Heterozygous mice ($Gnrhr^{Ctail/+}$) were interbred to produce wild-type (WT, $Gnrhr^{+/+}$), heterozygous ($Gnrhr^{Ctail/+}$), and homozygous (Ctail, $Gnrhr^{Ctail/Ctail}$) animals, which were born at the expected Mendelian frequencies (Figure 1-figure supplement 1C). Ctail mice expressed an mRNA encoding the chimeric receptor in their pituitaries (Figure 1-figure supplement 1D).

Ctail mice are hypogonadal and subfertile

We assessed the reproductive function of female and male Ctail mice relative to their WT littermates. When paired with WT C57BL/6 males, Ctail females produced smaller litters than WT (Figure 1A). A minority of Ctail mice were profoundly subfertile or infertile. Ctail females exhibited fewer estrous cycles per week (Figure 1B), due to an extended amount of time spent in estrus (Figure 1-figure supplement 2). Ovarian mass was reduced in Ctail females relative to WT

(Figure 1C-D), but uterine weight was not significantly altered (Figure 1E). The numbers of antral follicles (Figure 1F), preovulatory follicles (Figure 1G), and corpora lutea (Figure 1H) were reduced in Ctail relative to WT ovaries, indicating impairments in folliculogenesis and ovulation. Ctail males were hypogonadal (Figure 1I-J) and oligozoospermic (Figure 1K), but their seminal vesicle masses were comparable to those of WT (Figure 1I,L).

Serum FSH levels are reduced in Ctail mice

To help explain the observed hypogonadism in Ctail mice, we next examined gonadotropin secretion. In females sampled on diestrus afternoon, serum FSH and LH levels did not differ significantly (two-way ANOVA) between genotypes ('sham' data in Figure 2A-B), though there was a clear trend for reduced FSH in Ctail mice. Indeed, the difference was significant when analyzed directly after the removal of the confirmed outlier in the WT group [$t(19)=2.1$, $p=0.0012$, two-tailed]. A second cohort of females was ovariectomized (OVX) to remove gonadal hormone (steroids and inhibin) feedback and increase endogenous GnRH secretion. Under these conditions, FSH and LH levels increased, as expected (Figure 2A-B). There was no significant genotype difference observed, but both gonadotropins trended lower in OVX Ctail relative to WT females.

In males, serum FSH levels were significantly reduced in gonad-intact ('sham') Ctail relative to WT mice (Figure 2C). In contrast, both single time point (Figure 2D) and pulsatile LH release were statistically normal in Ctail males (Figure 2-figure supplement 1). FSH levels did not increase post-castration, but the difference between genotypes persisted (Figure 2C). The post-castration increase in LH levels was blunted in Ctail relative to WT males (Figure 2D).

Pituitary gonadotropin subunit and Gnrhr mRNA levels are altered in Ctail mice

To better understand the reduced gonadotropin levels in Ctail mice, we evaluated pituitary gonadotropin subunit (*Fshb*, *Lhb*, and *Cga*) and *Gnrhr* expression. In gonad-intact ('sham') animals, *Fshb* mRNA levels were significantly reduced in male, but not in female Ctail relative to WT mice (Figure 3A,E). Following gonadectomy, *Fshb* mRNA levels were increased in both genotypes, but the response was blunted in Ctail mice, significantly so in males (with a clear trend in females) (Figure 3A,E). Similar to serum LH levels, pituitary expression of the *Lhb* and *Cga* subunits did not differ between gonad-intact WT and Ctail males and females (Figure 3B-C, F-G). In contrast, following gonadectomy, increases in *Lhb* and *Cga* expression were significantly

blunted in Ctail mice (Figure 3B-C, F-G), paralleling the observed effects on LH secretion (Figure 2B,D). *Gnrhr* mRNA expression was significantly reduced in gonad-intact female and male Ctail relative to WT mice (Figure 3D,H). Following gonadectomy, the difference between genotypes was no longer statistically significant, but levels continued to trend lower in Ctail mice.

The preovulatory LH surge is blunted in female Ctail mice

GnRH secretion is increased post-gonadectomy (because of the loss of steroid negative feedback) and at the time of the LH surge (because of steroid positive feedback). Given impairments in LH production and/or release in gonadectomized Ctail mice, we next examined the naturally occurring preovulatory surge on the afternoon of proestrus. Five of eight WT females (62.5%) exhibited clear LH surges, while no Ctail mice (0% of N = 7) surged on proestrus, as determined by vaginal smearing (Figure 4A-B). As estrous cyclicity was altered in Ctail mice, we reasoned that we might have missed surges that actually occurred. Therefore, we took a different approach to assess natural LH surges, which previously proved successful in our assessment of LH surges in gonadotrope-specific progesterone receptor knockouts (42). Blood samples were collected four times daily over 11 consecutive days. Over the sampling interval, we detected LH surges in 93% of WT mice compared to 43% of Ctail animals (Figure 4C and Figure 4-figure supplement 1). The maximal LH levels measured were significantly blunted in Ctail relative to WT females (Figure 4C). The timing of the surge did not appear to differ between genotypes (Figure 4-figure supplement 1).

LH release is impaired in Ctail mice following GnRH stimulation

Blunted LH release both post-gonadectomy and during the proestrus surge suggested that GnRH action in gonadotropes might be altered in Ctail mice. To more directly assess GnRH responsiveness, we performed GnRH stimulation tests *in vivo.* Mice of both genotypes released LH in response to exogenous GnRH, with peaks observed 15 minutes post-injection and returning to baseline by 1 hour (Figure 5A,D). However, the amplitude of the response was blunted in Ctail relative to WT mice. Intra-pituitary FSH and LH levels were lower in female Ctail relative WT littermates (Figure 5B-C). In contrast, in males, pituitary FSH content did not differ between genotypes (Figure 5E), but pituitary LH content was slightly higher in Ctail than WT males (Figure 5F).

GnRH activation of $G\alpha_{q/11}$ via the Ctail receptor is impaired in vitro

The reductions in FSH production under basal conditions and in LH release when GnRH secretion was enhanced suggested that GnRH signaling was somehow altered in gonadotropes of Ctail mice. The GnRHR is canonically coupled to $G\alpha_{q/11}$ (43). We therefore interrogated $G\alpha_{q/11}$-dependent signaling downstream of WT and Ctail forms of the murine GnRHR *in vitro*. As assessed using a $G\alpha_q$ BRET-based biosensor, GnRH-dependent $G\alpha_q$ activation was markedly attenuated in heterologous HEK 293 cells expressing the Ctail relative to WT GnRHR receptor (Figure 6A), even though cell surface expression of the two receptors was equivalent (Figure 6-figure supplement 1).

$G\alpha_{q/11}$ signaling is associated with activation of phospholipase C, which cleaves phosphatidylinositol 4,5-bisphosphate into diacylglycerol (DAG) and inositol 1,4,5-trisphosphate (IP_3). As revealed with a DAG BRET-based biosensor, GnRH-dependent DAG production was impaired in HEK 293 cells expressing the Ctail compared to WT receptor (Figure 6B). GnRH stimulation of IP_1 production (a surrogate for IP_3) was also significantly attenuated in HEK 293 cells expressing the Ctail GnRHR (Figure 6C).

GnRH-dependent calcium mobilization, but not ERK signaling, is impaired downstream of the Ctail receptor in HEK 293 cells

DAG, alone or in combination with calcium, activates protein kinase C isoforms (PKC) (44). PKC, in turn, activates mitogen activated protein kinase signaling (45). GnRH activation of the extracellular regulated kinase 1/2 (ERK1/2) pathway is particularly important for *Lhb* transcription (46-48). In the gonadotrope-like cell line, LβT2, GnRH induction of ERK1/2 phosphorylation (pERK1/2) is $G\alpha_q$- (Figure 7-figure supplement 1A-B) and PKC-dependent (Figure 7-figure supplement 1C-D) (49, 50), but calcium-independent (Figure 7-figure supplement 1E-F). In transfected HEK 293 cells, GnRH induced pERK1/2 equivalently via the WT and Ctail receptors (Figure 7A-B) and in both cases was PKC-dependent (Figure 7C-D). Although the Ctail receptor acquired the ability to recruit β-arrestin-1 (Figure 7-figure supplement 2A-B), GnRH activation of ERK1/2 signaling was arrestin-independent (Figure 7-figure supplement 2C-D).

GnRH induction of intracellular calcium mobilization, which depends on IP_3, was reduced in Ctail relative to WT GnRHR expressing cells (Figure 7E). This impairment was not caused by

the Ctail receptor's enhanced internalization, as the defect was not rescued in cells lacking arrestins (Figure 7-figure supplement 2E).

GnRH-dependent calcium signaling is altered in gonadotropes of GnRHR-Ctail mice

As the above analyses were conducted in heterologous cells, we next examined GnRH regulated calcium signaling in gonadotropes of adult male WT and Ctail mice using a whole pituitary *ex vivo* preparation (see Methods). As expected, the three well-characterized GnRH-induced calcium response patterns were observed in individual gonadotropes of WT mice (Figure 8A): oscillatory (Figure 8B), biphasic (Figure 8C-D), and transient (Figure 8E). In contrast, gonadotropes of Ctail mice showed more uniform responses to GnRH (Figure 8F), with extended oscillatory or biphasic patterns that were not seen in WT (Figure 8G-J). There was no significant difference in the area under the curve (AUC) between genotypes (Figure 8K), or the maximum intensity of response (MIF, Figure 8L); however, the number of peaks per cell was significantly higher in Ctail gonadotropes (Figure 8M). When we correlated the AUC with the MIF, we observed a difference in the mobilization of calcium between genotypes, with Ctail gonadotropes having lower amplitude but longer duration intracellular calcium elevations (Figure 8N). WT gonadotropes showed principally oscillatory or biphasic response patterns, whereas Ctail gonadotropes exhibited more extended responses (Figure 8O). The transient response pattern occurred in fewer than 1% of cells and therefore was not examined quantitatively.

We further examined calcium response patterns to repeated GnRH pulses. Gonadotropes of both genotypes responded to a second GnRH pulse, one hour after the first, with no evidence of desensitization in either case (Figure 8-figure supplement 1). Indeed, the responses to the second pulse were comparable to the first in terms of AUC (Figure 8-figure supplement 1B,E), MIF (Figure 8-figure supplement 1C,F), and oscillatory patterns (Figure 8-figure supplement 1G-M). Next, we asked to what extent the response patterns depended on influx of calcium via voltage-gated L-type channels. As expected, the L-type channel blocker nimodipine altered GnRH responses in gonadotropes of WT animals, reducing both the AUC and MIF, as previously reported in (51) (Figure 8-figure supplement 2A-C). Nimodipine also reduced AUC and MIF in gonadotropes of the Ctail mice (Figure 8-figure supplement 2D-F). GnRH-induced calcium oscillations observed in control gonadotropes were absent in the presence of nimodipine (Figure 8-figure supplement 2G-I). Interestingly, the prolonged GnRH-induced calcium oscillations (both

oscillatory and biphasic responses) were decreased considerably in nimodipine-treated Ctail gonadotropes and, in most cells, were no longer present (Figure 8-figure supplement 2J-N).

GnRH-induction of Fshb expression is dependent on intracellular calcium

The mechanisms through which GnRH induces *Fshb* expression are poorly understood. However, given the impairments in FSH production in Ctail mice (Figure 2 and 3) and altered profile of GnRH-induced calcium signaling via the Ctail receptor (Figure 7E and 8), we asked whether there is a role for calcium in GnRH regulation of *Fshb*. A single pulse of GnRH was sufficient to induce *Fshb*, but not *Lhb* mRNA levels in LβT2 cells (Figure 9A-B). This is not unlike the situation in GnRH-deficient mice (*hpg*), where once daily GnRH is sufficient to induce FSH but not LH production (52, 53). GnRH-induced *Fshb* expression in LβT2 cells was blocked by the calcium chelator, BAPTA-AM (Figure 9A), which did not affect basal *Lhb* mRNA levels (Figure 9B). Pulsatile GnRH is required for LH induction in GnRH-deficient mice (54). Pulsatile GnRH stimulated both *Fshb* and *Lhb* mRNA expression in LβT2 cells and these responses were blocked with BAPTA-AM (Figure 9C-D), but not nimodipine (Figure 9-figure supplement 1).

Not all C-tails impair Gα_q activation and calcium mobilization via chimeric GnRHRs

Finally, we asked whether the effects observed with the chicken Ctail on the murine GnRHR occur with other non-mammalian GnRHR C-tails. Therefore, we added C-tails from type II GnRHRs of *Xenopus laevis* (frog), *Anolis carolinensis* (lizard), or *Clarias garepinus* (catfish) to the murine GnRHR (Figure 10-figure supplement 1). The *Anolis* C-tail impaired GnRH-induced Gα_q activation and calcium mobilization in HEK 293 cells, as observed with the chicken C-tail (Figure 10A-B, black and purple). In contrast, GnRH signaled via the *Clarias* chimeric receptor in a manner indistinguishable from the WT murine GnRHR (Figure 10A-B, green and blue). Addition of the *Xenopus* C-tail modestly attenuated GnRH-induced Gα_q activation but had no effect on calcium mobilization (Figure 10A-B, pink). GnRH effectively induced ERK1/2 phosphorylation via all of the chimeric receptors in a PKC-dependent manner (Figure 10C-D).

DISCUSSION

The loss of the carboxy-terminal tail from the GnRH receptor during mammalian evolution was previously hypothesized to be an adaptation that enabled pre-ovulatory LH surges (36, 55).

The data presented here challenge this idea. Addition of the chicken GnRHR C-tail to the endogenous murine GnRHR blunted but did not block the LH surge. With few exceptions, females expressing the mouse-chicken chimeric GnRHR (GnRHR-Ctail) were fertile, but with smaller litter sizes compared to wild-type mice. Reductions in FSH rather than perturbations of the LH surge likely explain their subfertility. The FSH impairment appears to derive from alterations in GnRH-induced calcium signaling.

Effects of the chicken C-tail on gonadotropin synthesis and secretion

Serum FSH and pituitary *Fshb* mRNA levels are lower in GnRHR-Ctail than wild-type mice. In males, this is associated with small, but significant decreases in testis mass and spermatogenesis. There is a direct relationship between Sertoli cell number and spermatogenic potential (56). Sertoli cell number is regulated by FSH during early postnatal development in rodents (24, 57). Though we did not quantify Sertoli cells in GnRHR-Ctail males or their FSH levels prior to weaning, it seems likely that the FSH deficiency observed in adulthood also occurs earlier in life in these animals. Indeed, depleting FSH in young but not adult mice reduces testis size and sperm counts (24, 58). In females, reduced FSH levels are associated with decreased numbers of preovulatory follicles. Because most GnRHR-Ctail females exhibit LH surges and/or corpora lutea, it is clear that the majority could and did ovulate. Therefore, the most parsimonious explanation for the subfertility in these females is impaired follicle development secondary to FSH deficiency.

Though present, LH surges are altered in most GnRHR-Ctail females. Unfortunately, we were unable to fully characterize the nature of the changes, as we had difficulty capturing surges in these animals when sampled on presumptive proestrus. Therefore, we could not measure the dynamics (the precise time of onset, maximum amplitude, or duration) of their LH surges relative to those of wild-type mice. Nevertheless, with our modified sampling protocol, we did observe LH surges in GnRHR-Ctail females, which were reduced in amplitude. It is unlikely that this contributed to their subfertility, however, as there are several mouse models with reduced LH surge amplitudes that do not exhibit fertility defects [e.g., (42, 59)]. Moreover, the amplitude of the surge varies dramatically between mice within a given strain [(60) and our unpublished observations]. Though we only detected LH surges in ~50% of GnRHR-Ctail mice, it is unlikely that they were truly blocked or absent in half of the animals. In the fertility trial, only 1 of 8 animals was sterile.

Similarly, in only 1 of 6 GnRHR-Ctail mice did we fail to observe corpora lutea in their ovaries. Thus, the complete absence of LH surges appears to be a rare event in these mice, most likely explained by inadequate FSH-stimulated follicle development and estrogen positive feedback. The cause of the variable (and low) penetrance of the infertility phenotype is presently unclear, but the animals were notably on a mixed genetic background.

The blunted LH surges in GnRHR-Ctail mice may derive, at least in part, from homologous receptor desensitization. The effects of adding C-tails to mammalian GnRHRs have been thoroughly investigated *in vitro*. In most cases, these manipulations are associated with agonist-induced receptor phosphorylation, arrestin recruitment, and receptor internalization (34, 36, 55, 61, 62). We similarly observed that the mouse-chicken chimeric GnRHR used here acquired the ability to recruit arrestin in response to GnRH. It is therefore likely that GnRHR-Ctail is rapidly internalized in response to agonist, but we did not assess this directly. Though arrestin recruitment to the chimera's C-tail did not appear to explain the altered calcium signaling or retained ERK activation in HEK 293 cells, we acknowledge that multiple GPCR/arrestin conformations, including differences between the receptor core and/or C-tail, can have distinct functions (63-66). Regardless, if we were able to measure the duration of LH surges in GnRHR-Ctail females, we predict that it would be shorter than in wild-type mice. However, as most of these mice ovulated, the amplitude and duration of these surges were clearly sufficient. We recently reported that kisspeptin-54 induces surge-like LH release in juvenile mice. Although the duration of the LH increase is shorter than natural surges, these mice still ovulate efficiently (67). Thus, both the amplitude and duration of natural LH surges are greater than actually needed to induce ovulation in mice.

Effects of the chicken C-tail on GnRH signaling

The reductions in gonadotropin production in GnRHR-Ctail mice indicate that the addition of the chicken C-tail altered GnRH signaling. In heterologous HEK 293 cells, GnRH stimulation of calcium mobilization was greatly impaired downstream of GnRHR-Ctail. This, in turn, appeared to be explained by attenuated activation of $G\alpha_q$ and reduced agonist stimulated inositol phosphate production. As GnRH induction of *Fshb* mRNA expression in homologous LβT2 cells is calcium dependent (68), it is possible that FSH deficiency in GnRHR-Ctail mice may result from alterations in calcium signaling. In contrast, GnRH induction of ERK1/2 phosphorylation is intact

323 downstream of GnRHR-Ctail in HEK 293 cells. In gonadotropes, GnRH promotes ERK1/2
324 signaling via PKC, which in turn depends on diacylglycerol (DAG) more so than calcium (69).
325 Though GnRH induction of DAG production was attenuated downstream of GnRHR-Ctail in HEK
326 293 cells, it was sufficient to activate PKC-ERK1/2 signaling. As GnRH regulation of *Lhb*
327 expression is ERK1/2-dependent (46), this may help explain how LH production was relatively
328 unperturbed in gonad-intact GnRHR-Ctail mice.

329 The $G\alpha_q$ activation and, in particular, calcium mobilization impairments, downstream of
330 GnRHR-Ctail in heterologous cells do not fully recapitulate changes in GnRH signaling in
331 gonadotropes in GnRHR-Ctail mice. However, in both HEK 293 cells and gonadotropes, the
332 GnRHR-Ctail induced a more sustained calcium profile. Gonadotropes possess L-type calcium
333 channels, which are absent in HEK 293 cells (70, 71), though the latter do have endogenous
334 calcium currents (72). GnRH-induced calcium oscillations in gonadotropes reflect both
335 mobilization from ER stores and influx via voltage-dependent L-type channels. The calcium
336 signaling (and defects therein) that we examined in HEK 293 cells is limited to mobilization from
337 internal stores. Nevertheless, it is evident that GnRH-induced calcium oscillations also differ
338 between gonadotropes of wild-type and GnRHR-Ctail mice. In wild-type pituitaries, we observe
339 the previously reported heterogeneity of responses: oscillatory, biphasic, and transient (73). In
340 contrast, GnRH stimulates a more homogenous calcium response in gonadotropes of GnRHR-
341 Ctail mice and one that is not observed in wild-type animals. Relative to wild-type, gonadotropes
342 of GnRHR-Ctail mice show sustained calcium oscillations, which extend well after the GnRH
343 pulse. The mechanisms underlying this sustained activity are not clear but depend to some extent
344 on influx of calcium via L-type channels. Regardless, the changes in calcium signaling from
345 primarily transient intracellular release of calcium to a sustained influx of extracellular calcium
346 may contribute to the observed reductions in FSH synthesis in GnRHR-Ctail mice.

347 In contrast, pulsatile LH secretion, which depends upon GnRH-induced calcium
348 mobilization (74), appears to be intact in GnRHR-Ctail males [note that we did not measure
349 pulsatile LH secretion in females because of the high variability between estrous cycle stages (60)
350 and the estrous cycle irregularities in GnRHR-Ctail mice]. This 'normal' LH secretion may be
351 more apparent than real, however. Exogenous GnRH stimulates less LH secretion in male GnRHR-
352 Ctail than wild-type mice, despite their equivalent pituitary LH contents. GnRH is similarly less
353 effective in stimulating LH release in GnRHR-Ctail females, but they also show marked decreases

in pituitary LH content relative to wild-type, precluding a definitive interpretation of the results. LH secretion is blunted in both sexes following gonadectomy and at the time of the LH surge in females. Therefore, the alterations in GnRH stimulated calcium signaling may also affect LH secretion, which is most evident when GnRH pulse frequency or amplitude is enhanced.

It is possible that the phenotypes of GnRHR-Ctail mice are explained by reduced receptor expression rather than (or in additional to) altered receptor function. Indeed, *Gnrhr* mRNA levels are reduced in gonad-intact GnRHR-Ctail relative wild-type mice. We do not know if this translates into differences in GnRHR protein expression. Unfortunately, we were unable to identify reliable antibodies for measurement of GnRHR protein in the pituitary. We also could not validate GnRHR ELISAs used by others (75) (data not shown). *In vitro* ligand binding assays in pituitaries from the two genotypes do not provide a viable alternative means for receptor protein quantification, as *Gnrhr* mRNA levels decrease dramatically in cultured cells relative to *in vivo* and the genotype difference in *Gnrhr* expression does not persist in culture (data not shown). Regardless, we hypothesize that the reduced *Gnrhr* mRNA levels in GnRHR-Ctail mice are themselves a consequence rather than a cause of altered GnRH signaling. Not only does GnRH positively regulate the expression of its own receptor (76, 77), but the wild-type and Ctail forms of the murine GnRHR are expressed at equivalent levels when transfected in heterologous cells. Thus, there does not appear to be any inherent difference in the stability of wild-type and Ctail forms of the receptor.

Evolutionary significance of the loss of the C-tail

Finally, in light of all of the results, it is tempting to speculate that the loss of the C-tail from the mammalian GnRHR may have conferred a selective advantage by augmenting G protein coupling, leading to enhanced calcium mobilization, FSH production, folliculogenesis, and fertility. However, more recent phylogenetic analyses suggest that the loss of the C-tail may be an ancient event in jawed vertebrates, predating mammalian evolution (40). It is unclear what advantage this may have conferred when it first emerged and why it has only been retained in mammals and a small number of other vertebrates. We are limited in what we can conclude or interpret from the one mouse model we examined here. While adding the chicken C-tail decreased FSH production, this may not have been the case if we had instead fused the *Xenopus* or *Clarias* C-tails, which do not appear to perturb GnRH signaling *in vitro*. Therefore, the presence of a C-

tail, in and of itself, does not necessarily impair or alter G protein coupling to the GnRHR. The specific sequence of the tail is relevant. It could be informative to reconstruct ancestral GnRHRs (78) and then examine the effects of removing their C-tails on signaling. Though challenging, this may ultimately provide more, or at least parallel, insight into the potential adaptive significance of the loss of the C-tail. Regardless, the data presented here demonstrate that LH surges are possible in mammals in the presence of a GnRHR with a disruptive C-tail and suggest that FSH synthesis is dependent upon the nature of GnRH-dependent calcium signaling in gonadotropes.

MATERIALS AND METHODS

Reagents

GnRH (LH releasing hormone, L7134), nimodipine (66085-59-4), paraformaldehyde (PFA, 158127), bovine serum albumin fraction V (BSA, 10735078001), Triton X-100 (9002-93-1), dimethyl sulfoxide (DMSO, 472301), anti-Flag antibody (F7425), EZview™ Red ANTI-FLAG® M2 Affinity Gel (F2426), and 3X FLAG® Peptide (F4799) were obtained from Sigma Aldrich (St-Louis, Missouri, USA). The PKC inhibitor Gö6983 (ab144414) was from Abcam (Cambridge, UK). BAPTA-AM (126150-97-8) was from Tocris (Bristol, UK). TRIzol reagent (15596026) was from Life Technologies (Carlsbad, CA, USA). ProLong Gold antifade (P36931), Pluronic F-127 20% solution (P3000MP), and Fluo4-AM (F1420) were from Thermo Fisher Scientific (Waltham, Massachusetts, USA). Deoxynucleotide triphosphates (dNTPs, 800-401-TL), fetal bovine serum (FBS, 080150), and DMEM (319-005-CL) were from Wisent Inc. (St-Bruno, QC, Canada). Oligonucleotides were synthesized by Integrated DNA Technologies (Coralville, IA, USA). Polyethylenimine (PEI, 23966) was from Polysciences Inc. (Warrington, PA, USA). Coelenterazine cp (10112) and coelenterazine 400a (10125) were from Biotium (Fremont, CA, USA). Phospho-p44/42 MAPK (Thr202/Tyr204 pERK1/2; 9101S) and p44/42 MAPK (ERK1/2; 9102S) antibodies were from Cell Signaling Technologies (Danvers, MA, USA). HRP-conjugated goat anti-rabbit (170-6516) and anti-mouse (170-6515) antibodies were obtained from BioRad Laboratories (Hercules, CA, USA).

Cell lines and transfections

LβT2 cells (79) were provided by Dr. Pamela Mellon (University of California, San Diego, CA, USA). HEK 293 wild-type (WT) and *Arrb1;Arrb2* CRISPR knockout (KO) cells were provided by Dr. Inoue Asuka [Tokyo University, Sendai, Japan; (80)]. All cells were maintained and grown in DMEM (4.5 g/L glucose, with L-glutamine and sodium pyruvate) containing 10% (v/v) FBS at 37°C in a 5% CO_2 atmosphere. Transfections of HEK 293 cells lines were performed using PEI transfection reagent in a mass ratio of 3:1 PEI to DNA.

Plasmids

pGEM-T Easy was purchased from Promega (Wisconsin, USA; Cat # A1360). To generate the flag-tagged murine GnRHR-WT and GnRHR-Ctail expression vectors, the murine *Gnrhr* coding sequence was amplified by PCR from LβT2 cell cDNA using a forward primer introducing an *Eco*RI restriction site and omitting the endogenous translation initiation codon and a reverse primer introducing an *Xba*I restriction site (Table 1). The resulting fragment was digested with the indicated enzymes and ligated in-frame downstream of the flag tag coding sequence preceded by a translation initiation codon in pcDNA3.0, yielding Flag-GnRHR. To generate the Flag-GnRHR-Ctail vector, the stop codon in Flag-GnRHR was replaced with a *Cla*I restriction site by site-directed mutagenesis (QuikChange protocol). The C-tail coding sequence from the chicken *Gnrhr* gene (*Gallus gallus*; NP_989984) was amplified by PCR from chicken embryonic genomic DNA (provided by Dr. Aimee Ryan, McGill University) using primers incorporating *Cla*I sites at both ends (Table 1). This fragment was inserted into the *Cla*I site created at the end of the *Gnrhr* coding sequence.

To generate other chimeric receptors, the C-tail coding sequence from the frog *Gnrhr* gene (*Xenopus leavis*; accession number NM_001085707) was PCR amplified from HA-XGnRHR [(81); provided by Dr. Craig McArdle, University of Bristol, Bristol, UK] using primers incorporating *Cla*I sites at both ends (Table 1), replacing the amino acids underlined in Figure 10-figure supplement 1). C-tail coding sequences from the *Gnrhr* of the lizard *Anolis carolinensis* (XP_003226613.1) and from the catfish *Clarias gariepinus* (adapted from the coding sequence of *Tachysaurus fulvidraco Gnrhr* [XM_027175679.1] based on the peptide sequence described in (62)) were synthesized as double stranded DNA by Twist Biosciences (San Francisco, CA), harboring *Cla*I sites downstream of adaptors added at both ends. These C-tails were PCR

amplified using primers complementary to the adaptor sequences (Table 1), digested with *Cla*I, purified, and ligated into *Cla*I-digested dephosphorylated Flag-GnRHR-Ctail, from which the chicken C-tail was excised. All clones were confirmed by Sanger sequencing at GenomeQuébec, Montreal, Canada.

The polycistronic $G\alpha_q$ (82) and DAG (83) biosensors, and β-arrestin-1-YFP (84) constructs were provided by Dr. Stéphane Laporte (McGill University, Montréal, Canada). The luminescence obelin biosensor (85) was provided by Dr. Michel Bouvier (Université de Montréal, Canada).

Targeting vector

To generate the downstream chromosomal arm (DCA), a 6.7 kb DNA fragment starting 1 kb upstream of murine *Gnrhr* exon 3 was amplified by PCR using the Expand Long Template PCR System (Roche, Basel, Switzerland) from 129SvEv genomic DNA using primers incorporating 5' *Xma*I and 3' *Not*I restriction enzyme sites (Table 1). The fragment was cloned into pGEM-T Easy. The stop codon in exon 3 was replaced with a *Cla*I restriction enzyme site by site-directed mutagenesis. The *Cla*I-flanked C-tail coding sequence from the chicken *Gnrhr* (also used for the Flag-GnRHR-Ctail construct described above) was inserted, and the correct orientation was verified by sequencing. The whole DCA containing the chimeric exon 3 was ligated between the *Xma*I and *Not*I sites in pKOII (86), 3' of the *Frt* flanked neomycin (neo) selection cassette. We used a two-step process to generate the upstream chromosomal arm (UCA) and the "floxed" exon 3 regions. First, a genomic DNA fragment starting 1 kb upstream of exon 3 and terminating immediately after the stop codon in exon 3 was amplified by PCR using a 5' primer introducing a *Xma*I restriction site and a *loxP* site, and a 3' primer introducing a *Pme*I restriction site (Table 1). This amplicon, along with a *Pme*I-*Xho*I fragment comprising the bovine growth hormone (BGH) polyA sequence (obtained by PCR from the pcDNA3.0 expression vector) were ligated in a 3-part ligation between the *Xma*I and *Xho*I restriction sites of pBluescript II KS. To complete the UCA, a 3.6 kb fragment spanning exon 2 and terminating 1 kb upstream of exon 3 (the position of the upstream *loxP* site) was amplified by PCR using primers incorporating 5' *Kpn*I and 3' *Xma*I sites (Table 1) and joined to the *Xma*I-*Xho*I construct (in pBluescript II KS) described above. The whole UCA was then ligated into the *Kpn*I and *Xho*I restriction sites in the pKOII vector containing the DCA, 3' of the diphtheria toxin A (DTa) negative selection cassette. Sequencing was performed to ensure the integrity of the targeting vector and the absence of

476 mutations in and around exons and splice-junctions (GenomeQuébec, Montreal, Canada). The
477 targeting vector was linearized with *Kpn*I, phenol-chloroform extracted, and resuspended at a final
478 concentration of 1 µg/µl in Tris-EDTA.
479
480 *Generation of mice*
481 Twenty-five µg of linearized targeting vector were electroporated into 10 million R1 ES cells
482 (129/SvEv-derived) in triplicate, and each electroporated sample plated on primary mouse
483 embryonic fibroblasts in two 10-cm dishes. The following day, culture media was supplemented
484 with 200 µg/mL G418 for positive selection of clones incorporating the targeting vector. After 8
485 days of selection, 420 clones were picked manually under a dissecting microscope, dissociated in
486 trypsin, and transferred to individual wells of 96-well plates. Cells were cultured for 5 days and
487 then split into three separate plates. Two plates were frozen at -80°C after the addition of 10%
488 DMSO. Cells in the remaining plate were grown to confluence. Genomic DNA was extracted,
489 cleaned with a series of 75% ethanol washes and digested overnight with *Xma*I. Homologous
490 recombination events were screened by Southern blot using sequential hybridization with 5' and
491 3' probes external to the homology arms (see Table 1 for the primers used to generate the probes).
492 C57BL/6J blastocysts were microinjected with cells from two correctly targeted clones and
493 transferred into pseudopregnant mothers at the Transgenic Core Facility of the Life Science
494 Complex at McGill University. Resulting chimeric males were bred to C57BL/6J females and
495 germline transmission of ES cell-derived DNA monitored by coat color. Brown pups were
496 genotyped by PCR for the presence of the modified allele (denoted *Gnrhr*$^{\text{CtailfloxNeo}}$) and later
497 confirmed by Southern blot. The Neo cassette was removed *in vivo* by breeding *Gnrhr*$^{\text{CtailfloxNeo/+}}$
498 mice to "flp deleter" mice [*B6.129S4-Gt(ROSA)26Sor*$^{tm1(FLP1)Dym}$*/RainJ*, obtained from The
499 Jackson Laboratory (87)]. The resulting *Gnrhr*$^{\text{Ctailflox/+}}$ mice were bred to *EIIa::Cre* transgenic
500 mice [*B6.FVB-Tg(EIIa-cre)C5379Lmgd/J*, obtained from the Jackson Laboratory (88)] to yield
501 *Gnrhr*$^{\text{Ctail/+}}$ mice (genotyped using primers Exon3 and Exon3-Ctail in Table 1). *Gnrhr*$^{\text{Ctail/+}}$ females
502 and males were then crossed to generate wild-type (WT; *Gnrhr*$^{+/+}$) and Ctail (*Gnrhr*$^{\text{Ctail/Ctail}}$) mice.
503 Genotyping was verified by PCR using the gDNA *Gnrhr* primers (Table 1). All animal
504 experiments in Canada were performed in accordance with institutional and federal guidelines and
505 were approved by the McGill University Facility Animal Care Committee (DOW-A; protocol
506 5204). Mice were maintained on a 12:12 light/dark cycle (on/off at 7:00 AM/7:00 PM) and fed

ad libitium. Mouse studies conducted at the National University of Mexico were performed under an institutional protocol similar to the United States Public Health Service Guide for the Care and Use of Laboratory Animals, and according to the Official Mexican Guide from the Secretary of Agriculture (SAGARPA NOM-062-Z00-1999).

Estrous cycle staging and fertility assessment

Estrous cyclicity was assessed in 6-week-old mice for 21 consecutive days as described in (89). At nine weeks of age, females were paired with WT C57BL/6 males (Charles River, Senneville, QC, Canada) for a six-month period. Breeding cages were monitored daily and the frequency of delivery and number of pups per litter were recorded. Pups were removed from cages 14 days after birth.

Reproductive organ analyses, gonadal histology, and sperm counts

Testes, seminal vesicles, ovaries, and uteri were collected from 10- to 12-week-old males and females (diestrus afternoon). Body and organ masses were measured on a precision balance. Ovaries were fixed in 10% formalin, paraffin-embedded, and sectioned continuously at 5-µm thickness per section. Sections mounted on slides and then stained with hematoxylin and eosin for antral follicle (AF), preovulatory antral (Graafian) follicle (POF), and corpora lutea (CL) counting as described in (90). For sperm counts, testes were homogenized in 10% DMSO in 1X PBS using a Polytron PT10-35. Heads of mature spermatozoa were counted using a Leica DM-1000 microscope (Leica Microsystems, Wetzlar, Germany).

Gonadectomy

Ovariectomy (OVX), castration (Cast), and sham operations were performed on 10-week-old mice following McGill University standard operating procedures #206 and #207 (https://www.mcgill.ca/research/research/compliance/animals/animal-research-practices/sop) respectively, as described in (91).

Blood collection

Blood was collected by cardiac puncture two weeks post-operatively (on diestrus afternoon for sham-operated females). Blood was allowed to clot for 30 min at room temperature and

538 centrifuged at 1000 g for 10 min to collect serum. Sera were stored at -20°C until hormone assays
539 were performed. For LH pulsatility assessment in 10-week-old males, 2 µl of blood were collected
540 from the tail tip every 10 min over 6 hours, starting 3 hours before lights off. For the LH surge
541 onset and profile in 10-week-old females, 2 µl of blood were collected from the tail tip every 20
542 min over 8 hours on proestrus (as assessed by vaginal cytology). For LH surge amplitude
543 assessment, four blood samples (4 µl each) were collected from the tail tip over 11 consecutive
544 days: at 10:00 AM, and at 6:00, 7:00 and 8:00 PM. The surge amplitude was defined as the
545 maximal concentration of LH measured on days determined to be proestrus by vaginal smears. For
546 the GnRH-induced LH release experiment, 4 µl of blood were collected from the tail tip of 10-11-
547 week-old females (diestrus afternoon) and males just prior to and 15- , 30- , and 60-minutes post-
548 i.p. injection of either 0.25 ng (males only), 0.75 ng (females only), or 1.25 ng of GnRH per g of
549 body mass, diluted in 0.9% NaCl. Prior to all tail tip blood collection, animals were acclimatized
550 by massaging the tail daily for two weeks. Tail tip blood samples for LH analysis were immediately
551 diluted (1:30) in 1X PBS containing 0.05% Tween (PBS-T), gently vortexed, and placed on dry
552 ice. Diluted blood was stored at -80°C until assayed.
553
554 *Hormone analyses*
555 Serum FSH and LH levels were determined in males at the Ligand Assay and Analysis Core
556 at the University of Virginia Center for Research in Reproduction using the mouse/rat LH/FSH
557 multiplex assay (detection limit: 2.4 to 300 ng/mL; intra-assay CV < 10%). In females, serum FSH
558 was measured by the MILLIPLEX kit (MPTMAG-49K, Millipore, Massachusetts, USA)
559 following the manufacturer's instructions (minimal detection limit: 9.5 pg/mL; intra-assay CV <
560 15%) and serum LH was measured using an in-house sandwich ELISA, as previously described
561 (92) (detection limit: 0.117 to 30 ng/mL; and intra-assay CV < 10%). Whole blood LH levels from
562 both males and females were also measured using the in-house sandwich LH ELISA.
563
564 *Gonadotropin pituitary content assessment*
565 Pituitaries were collected from 12- to 13-week-old female (randomly cycling) and male
566 mice, placed on dry ice, and manually homogenized in 300 µl cold 1X PBS. Homogenates were
567 centrifuged at 13,000 rpm for 15 minutes at 4°C. Total protein concentration was measured using

568 the Pierce BCA Protein Assay Kit (23225; ThermoFisher Scientific) following the manufacturer's
569 instructions.
570 For FSH content assessment, samples were diluted 1:50 and FSH levels were measured by
571 the MILLIPLEX kit (females) or by RIA (males) at the Ligand Assay and Analysis Core at the
572 University of Virginia Center for Research in Reproduction. For LH pituitary content, samples
573 were diluted 1:1,000,000 in PBS-T, and LH levels were measured using the LH ELISA indicated
574 above. FSH and LH values were normalized over total protein content per pituitary.
575
576 *GnRH treatment of LβT2 cells*
577 LβT2 cells were plated at 650,000 cells/well in 12-well plates and cultured overnight. The
578 next day, cells were starved for 16-18 hours in serum-free medium. Cells were then pre-treated for
579 20 minutes with BAPTA-AM (20 μM) and then stimulated with one pulse of 10 nM GnRH
580 (hereafter referred to as low GnRH pulse frequency). Two hours post-GnRH stimulation, media
581 was replaced with fresh media containing the BAPTA-AM and incubated for an additional 2 hours.
582 For high GnRH pulse frequency treatment, cells were stimulated with 10 nM GnRH for 5 min,
583 every 45 minutes for a total of 10 pulses in the presence of the BAPTA-AM (20 μM) or vehicle.
584 The latter were also included between GnRH pulses.
585
586 *Reverse transcription and quantitative PCR*
587 Pituitaries were collected two weeks post-gonadectomy (on diestrus afternoon for sham-
588 operated females), snap-frozen in liquid nitrogen, and stored at -80°C. Total RNA from pituitaries
589 and LβT2 cells was isolated with TRIzol following the manufacturer's instructions. Pituitaries
590 were first homogenized in 500 μl TRIzol using a Polytron PT10-35 homogenizer. RNA
591 concentration was measured by NanoDrop and 250 ng of RNA per sample were reverse transcribed
592 as in (93). Two μl of cDNA were used as a template in 20 μl reactions for quantitative-real time
593 PCR analysis on a Corbett Rotorgene 600 instrument (Corbett Life Science) using EvaGreen
594 reagent master mix. Relative gene expression was determined using the $2^{-\Delta\Delta Ct}$ method (94) with
595 the housekeeping gene ribosomal protein L19 (*Rpl19*) as reference (primers in Table 1).
596

Bioluminescence resonance energy transfer (BRET) assays

HEK 293 cells were plated at a density of 400,000 cells/well in 6-well plates. The next day, cells were co-transfected with PEI with 1 µg GnRHR-WT or GnRHR-Ctail expression vector (or empty vector as control) along with 1 µg of a polycistronic $G\alpha_q$ biosensor (95) or DAG biosensor (83). Twenty-four hours post-transfection, cells were detached by manual pipetting, and plated on poly-D-lysine-coated 96-well white plates at a density of 50,000 cells per well. The next day, cells were washed twice with Tyrode's buffer (140 mM NaCl, 1 mM $CaCl_2$, 2.7 mM KCl, 0.49 mM $MgCl_2$, 0.37 mM NaH_2PO_4, 5.6 mM glucose, 12 mM $NaHCO_3$, and 25 mM HEPES, pH 7.5). Next, cells were loaded with 5 µM Coelenterazine 400a for 5 min in the dark at room temperature, and signals were subsequently recorded by a Victor X light plate reader (Perkin Elmer Life Sciences) starting 10 seconds before and continuing 30 seconds after 100 nM GnRH (or vehicle) injection, at 0.33 millisecond intervals. Net BRET was calculated as the ratio of the acceptor signal (GFP10 515/30 nm filter) over the donor signal (RLucII, 410/80 nm filter). ΔBRET was calculated by subtracting the average of basal BRET signals from ligand-induced signals (96). Experiments with the $G\alpha_q$ biosensor and *Anolis*, *Xenopus*, and *Clarias* chimeric receptors were conducted as above, with the exception that a Synergy 2 Multi-Mode Microplate Reader (Bio Tek) was employed. Acceptor and donor signals were read three times before and after 100 nM GnRH (or vehicle) injection, at 16 s intervals.

Cell line protein extraction, immunoprecipitation, and western blotting

Cellular extracts from HEK 293 and LβT2 cell lines were isolated using RIPA lysis buffer (50 mM Tris-HCl, 150 mM NaCl, 10 mM EDTA, 1% Triton X-100) as described in (97). Total protein concentration was measured using the Pierce BCA Protein Assay Kit (23225; ThermoFisher Scientific) following the manufacturer's instructions. Fifteen to 30 µg of total protein extracts were resolved by 10% SDS-PAGE, and transferred onto nitrocellulose membranes (1060001, GE Healthcare). Membranes were blocked for 1 hour at room temperature with blocking solution [Tris-buffered saline with 0.05% Tween (TBS-T) containing 5% skim milk]. To investigate ERK1/2 phosphorylation, membranes were probed with rabbit anti-phospho-ERK1/2 (1:1000) for 16-18 hours at 4°C. For receptor expression, extracts were first incubated with EZview™ Red ANTI-FLAG® M2 Affinity Gel and eluted with 3X FLAG peptide following manufacturer's instructions. Membranes were incubated with rabbit anti-Flag (1:1000). Following

628 3 washes with TBS-T, membranes were further incubated with horseradish peroxidase (HRP)-
629 conjugated goat anti-rabbit antibody (1:5000) in blocking solution for 2 hours at room temperature.
630 For assessment of total ERK1/2 expression, membranes were stripped with 0.3 M NaOH, washed
631 and incubated with anti-ERK1/2 (1:1000) following the same procedure as above for phospho-
632 ERK1/2. Blots were incubated in Western Lightning ECL Pro reagent (Perkin Elmer) and then
633 exposed on HyBlot CL film (E3012, Denville Scientific) or with a digital GE Amersham Imager
634 600. Band intensities were measured in arbitrary units using Image J software (US National
635 Institutes of Health, Bethesda, Maryland). Phosphorylated-ERK1/2 values were normalized over
636 total ERK1/2 values in the same lane.
637
638 *IP1 production*
639 HEK 293 cells were seeded at 400,000 cells/well in 6-well plates. The next day, cells were
640 transfected with 1 μg of GnRHR-WT or GnRHR-Ctail expression vectors using PEI transfection
641 reagent in a mass ratio of 3:1 PEI to DNA. Twenty-four hours post-transfection, cells were
642 detached by manual pipetting and re-plated in 384-well low volume white plates (15,000
643 cells/well) and incubated for an additional 24 hours. Next, cells were washed and stimulated with
644 0, 10, or 100 nM GnRH for 30 min at 37°C. IP1 production was assessed using IP-ONE-Gq Kit
645 (Cisbio, Codolet, France) following the manufacturer's instructions. Homogeneous Time-
646 Resolved Fluorescence (HTRF) was measured using a Synergy 2 Multi-Mode Microplate Reader
647 (BioTek) and the ratio was calculated following the manufacturer's instructions. Data are
648 presented as relative HTRF, where values of stimulated conditions were normalized over the value
649 of untreated GnRHR-WT expressing cells.
650
651 *Intracellular calcium mobilization in heterologous cells*
652 HEK 293 cells were plated at a density of 400,000 cells/well in 6-well plates. The next day,
653 cells were co-transfected with 1 μg of GnRHR-WT receptor or the indicated chimeric receptor
654 expression vectors (or empty vector as control), and 1 μg Obelin biosensor, using PEI transfection
655 reagent in a mass ratio of 3:1 PEI to DNA. Twenty-four hours post-transfection, cells (10^6/ml)
656 were washed with phenol-free, serum-free DMEM supplemented with 0.1% BSA (media),
657 detached manually, and loaded with media containing 5 mM of Coelenterazine cp for two hours,
658 shaking in the dark, at room temperature. Subsequently, 50,000 cells (in 50 μl) were plated per

well in 96-well white microplates and 100 nM of GnRH (or vehicle) were injected using Synergy 2 Multi-Mode Microplate Reader (Bio Tek) or Victor X light plate reader (Perkin Elmer Life Sciences). Luminescence signals were recorded for 30 seconds, every 22 ms, and kinetic measurements were normalized over the maximal response (Lmax) obtained by lysing the cells with 0.1% Triton X-100.

Calcium imaging in pituitaries

Whole pituitaries were dissected and incubated (37°C, 95% O_2 and 5% CO_2) for 30 min with the calcium sensor Fluo 4AM (InVitrogen; Eugene, OR USA) at a final concentration of 22 µM in 0.1% DMSO (Sigma, St. Louis MO, USA), 0.5% pluronic acid F-127 (Sigma) in artificial cerebrospinal fluid (ACSF; 18 mM NaCl, 3 mM KCl, 2.5 mM $CaCl_2$, 25.2 mM $MgCl_2$, 2.5 mM $NaHCO_3$, 11 mM glucose and 1.1 mM HEPES). The pituitaries were immobilized in a drop of 3% agar and placed on top of a Plexiglas chamber, which was then attached to the microscope stage and was continuously perfused (2 mL/min) with ACSF at room temperature. The pituitary was positioned to enable visualization of the ventral surface of the gland.

Baseline activity was recorded for 3.5 min while the sample was perfused with ACSF. To evaluate GnRH effects, 1 min baseline activity was recorded, followed by application of 10 nM GnRH (LHRH acetate salt, BACHEM H-4005.0025 1062179; Bubendorf, Switzerland) for 30 s followed by a washout period with ACSF for 1.5 min. GnRH and ACSF solutions were directly applied to the recording chamber by a gravity-fed perfusion system.

To evaluate the contribution of voltage-gated calcium channels, after 1 h of recovery, tissue was incubated for 30 s with 20 µM nimodipine (ALOMONE LABS N-150 N150SM0250; Jerusalem, Israel) followed by a second application of 10 nM GnRH alone (Figure 8-figure supplement 1) or in combination with 20 µM nimodipine (Figure 8-figure supplement 2) for 30 s. Finally, to determine cell viability, high potassium solution (50 KCl mM, 120 NaCl mM, 10 HEPES mM, 2 $CaCl_2$ mM, pH 7.4) was applied for 30 s. For each condition, the numbers of animals and cells analyzed are indicated in the figure legends.

Image acquisition was performed with a cooled CCD camera (HyQ; Roper Scientific, Acton MA, USA); 600 images sequences were acquired with each image taken with 200 ms exposure. The tissue was viewed with an epifluorescence microscope (Leica M205FA; Leica Microsystem; Wetzlar, Germany) equipped with a PlanAPO 2.0% (0.35NA) objective lens. The excitation and suppression filters were BP 480/40 and BP 527/30, respectively.

690 Image sequences (1200 images; 200 ms-exposure) were obtained from a given field of
691 view, before, during, and after GnRH application and were saved in TIFF format. Movies were
692 processed and analyzed with ImageJ macros (NIH) to obtain numerical values of fluorescence
693 intensity corresponding to $[Ca^{2+}]i$ changes. Every responsive cell was selected manually from the
694 obtained recordings. Values of fluorescence were corrected for photobleaching and normalized
695 using Igor Pro (Wavemetrics Inc.; Portland, OR, USA) with a semi-automatic routine written by
696 Pierre Fontaneaud (Institute of functional Genomics, Montpellier, France) to obtain $\Delta F=F-F0$
697 values, which were then plotted with a routine written by Leon Islas, Ph.D. (Medicine Faculty,
698 UNAM, Mexico City) to visualize activity of each cell over time. GnRH responsive cells were
699 selected based on whether fluorescence values changed over time following ligand application.
700 All the cells analyzed responded to the depolarizing solution of high potassium.
701
702 *Immunofluorescence microscopy*
703 HEK 293 cells were plated on poly-D-lysine (1 mg/ml)-coated coverslips, placed in a 24
704 well plate. The next day, cells were transfected with 300 ng GnRHR-WT or GnRHR-Ctail along
705 with 200 ng of pYFP-Arrestin. Twenty-four to 48 hours post-transfection, cells were treated with
706 100 nM GnRH or 1 μM of the GnRH analog Lucrin for 1, 5, or 20 min or left untreated as control.
707 Cells were then fixed for 20 min with fresh 4% PFA and 0.2% Triton X-100. Coverslips were than
708 mounted on glass slides using ProLong Gold. Fluorescence images were acquired with a Leica
709 DM-1000 microscope with a 40X objective, or confocal microscope (Leica SP5) with a 63x 1.4
710 numerical aperture objective. Leica LAS AF image software was utilized for image acquisition.
711
712 *Cell surface expression with whole cell anti-Flag ELISA*
713 HEK 293T cells were plated at a density of 40,000 cell per well on poly-D-lysine (1 mg/ml)
714 coated 24-well plates. The next day, cells were transfected with 500 ng of empty vector, GnRHR-
715 WT, or GnRHR-Ctail using PEI transfection reagent in a mass ratio of 3:1 PEI to DNA. Forty-
716 eight hours post-transfection, cells were fixed with fresh PFA (4%) for 20 min, washed 3 times
717 gently with 1X PBS, and blocked for 2 hours with blocking solution (1X PBS containing 5% nonfat
718 milk and 5% goat serum). Cells were incubated with rabbit anti-flag antibody (1:5000 in blocking
719 solution) for 2 hours at room temperature. Next, cells were washed 3 times for 5 min each with 1X
720 PBS, and further incubated for 1 hour with HRP-conjugated goat anti-rabbit antibody (1:5000 in

721 blocking solution), followed by 5 washes for 5 min each with 1X PBS, and finally incubated in
722 500 µl of 3,3′,5,5′-Tetramethylbenzidine substrate for 15 min. The reaction was stopped by adding
723 2N sulfuric acid. Absorbance was measured at 450 nm using a Biochrom Asys UVM 340
724 microplate reader.
725
726 *Statistical analyses*
727 Statistical analyses were performed using GraphPad Prism software version 6 or 8 (San
728 Diego, California USA, www.graphpad.com), with the following exceptions. LH pulse data from
729 males were deconvoluted using MatLab. For whole-gland intracellular calcium experiments, the
730 area under the curve (AUC) and maximal intensity of fluorescence (MIF) from the normalized
731 values were extracted using R (version 3.5.1; https://www.R-project.org/) along with the following
732 packages: dplyr, pracma, ggplot2 and ggpubr. The number of oscillations in gonadotropes
733 identified with the oscillatory pattern of calcium mobilization was quantified automatically with
734 the MathLab-based toolbox PeakCaller (98). The statistical significance of AUC, MIF, and number
735 of oscillations (peaks) was tested in GraphPad using Wilcoxon rank-sum test when comparing
736 means of two groups, or Wilcoxon signed-rank test when comparing responses of one cell to two
737 stimuli. Statistical tests used, number of experiments, number of biological replicates, and p values
738 are indicated in the figure legends. Results were considered statistically significant when $p < 0.05$.
739
740 **ACKNOWLEDGEMENTS:**
741 We thank Dr. Aimee Ryan and Dr. Stéphane Laporte from McGill University, Canada; Dr.
742 Michel Bouvier from Institute for Research in Immunology and Cancer, Canada; Dr. Craig
743 McArdle from Bristol University, UK; Dr. Inoue Asuka from Tokyo University, Japan; Dr.
744 Pamela Mellon from University of California, USA for providing the indicated reagents.
745
746 **COMPETING INTERESTS:** There are no competing interests to disclose.
747

REFERENCES:

1. Whitlock KE, Postlethwait J, Ewer J. Neuroendocrinology of reproduction: Is gonadotropin-releasing hormone (GnRH) dispensable? Front Neuroendocrinol. 2019;53:100738.
2. Maggi R, Cariboni AM, Marelli MM, Moretti RM, Andre V, Marzagalli M, et al. GnRH and GnRH receptors in the pathophysiology of the human female reproductive system. Hum Reprod Update. 2016;22(3):358-81.
3. Brown JL, Roberson M. Novel Insights into Gonadotropin-Releasing Hormone Action in the Pituitary Gonadotrope. Semin Reprod Med. 2017;35(2):130-8.
4. Conn PM, McArdle CA, Andrews WV, Huckle WR. The molecular basis of gonadotropin-releasing hormone (GnRH) action in the pituitary gonadotrope. Biol Reprod. 1987;36(1):17-35.
5. Huirne JA, Lambalk CB. Gonadotropin-releasing-hormone-receptor antagonists. Lancet. 2001;358(9295):1793-803.
6. Huerta-Reyes M, Maya-Nunez G, Perez-Solis MA, Lopez-Munoz E, Guillen N, Olivo-Marin JC, et al. Treatment of Breast Cancer With Gonadotropin-Releasing Hormone Analogs. Front Oncol. 2019;9:943.
7. Corona SP, Roviello G, Strina C, Milani M, Allevi G, Aguggini S, et al. Could gonadotropin-releasing hormone analogs be helpful in the treatment of triple-negative breast cancer? Future Oncol. 2017;13(27):2473-7.
8. Bouligand J, Ghervan C, Tello JA, Brailly-Tabard S, Salenave S, Chanson P, et al. Isolated familial hypogonadotropic hypogonadism and a GNRH1 mutation. N Engl J Med. 2009;360(26):2742-8.
9. Wolczynski S, Laudanski P, Jarzabek K, Mittre H, Lagarde JP, Kottler ML. A case of complete hypogonadotropic hypogonadism with a mutation in the gonadotropin-releasing hormone receptor gene. Fertil Steril. 2003;79(2):442-4.
10. Costa EM, Bedecarrats GY, Mendonca BB, Arnhold IJ, Kaiser UB, Latronico AC. Two novel mutations in the gonadotropin-releasing hormone receptor gene in Brazilian patients with hypogonadotropic hypogonadism and normal olfaction. J Clin Endocrinol Metab. 2001;86(6):2680-6.
11. Topaloglu AK, Lu ZL, Farooqi IS, Mungan NO, Yuksel B, O'Rahilly S, et al. Molecular genetic analysis of normosmic hypogonadotropic hypogonadism in a Turkish population: identification and detailed functional characterization of a novel mutation in the gonadotropin-releasing hormone receptor gene. Neuroendocrinology. 2006;84(5):301-8.
12. Cattanach BM, Iddon CA, Charlton HM, Chiappa SA, Fink G. Gonadotrophin-releasing hormone deficiency in a mutant mouse with hypogonadism. Nature. 1977;269(5626):338-40.
13. Combarnous Y. Structure and structure-function relationships in gonadotropins. Reprod Nutr Dev. 1988;28(2A):211-28.
14. Pierce JG, Parsons TF. Glycoprotein hormones: structure and function. Annu Rev Biochem. 1981;50:465-95.
15. Cahoreau C, Klett D, Combarnous Y. Structure-function relationships of glycoprotein hormones and their subunits' ancestors. Front Endocrinol (Lausanne). 2015;6:26.
16. Thompson IR, Ciccone NA, Xu S, Zaytseva S, Carroll RS, Kaiser UB. GnRH pulse frequency-dependent stimulation of FSHbeta transcription is mediated via activation of PKA and CREB. Mol Endocrinol. 2013;27(4):606-18.
17. Thompson IR, Kaiser UB. GnRH pulse frequency-dependent differential regulation of LH and FSH gene expression. Mol Cell Endocrinol. 2014;385(1-2):28-35.

18. Kaiser UB, Jakubowiak A, Steinberger A, Chin WW. Differential effects of gonadotropin-releasing hormone (GnRH) pulse frequency on gonadotropin subunit and GnRH receptor messenger ribonucleic acid levels in vitro. Endocrinology. 1997;138(3):1224-31.
19. Loumaye E, Catt KJ. Homologous regulation of gonadotropin-releasing hormone receptors in cultured pituitary cells. Science. 1982;215(4535):983-5.
20. Hazum E, Keinan D. Photoaffinity labeling of pituitary gonadotropin releasing hormone receptors during the rat estrous cycle. Biochem Biophys Res Commun. 1982;107(2):695-8.
21. Clayton RN, Solano AR, Garcia-Vela A, Dufau ML, Catt KJ. Regulation of pituitary receptors for gonadotropin-releasing hormone during the rat estrous cycle. Endocrinology. 1980;107(3):699-706.
22. Layman LC. Mutations in the follicle-stimulating hormone-beta (FSH beta) and FSH receptor genes in mice and humans. Semin Reprod Med. 2000;18(1):5-10.
23. Abel MH, Wootton AN, Wilkins V, Huhtaniemi I, Knight PG, Charlton HM. The effect of a null mutation in the follicle-stimulating hormone receptor gene on mouse reproduction. Endocrinology. 2000;141(5):1795-803.
24. Kumar TR, Wang Y, Lu N, Matzuk MM. Follicle stimulating hormone is required for ovarian follicle maturation but not male fertility. Nat Genet. 1997;15(2):201-4.
25. Smith JT, Dungan HM, Stoll EA, Gottsch ML, Braun RE, Eacker SM, et al. Differential regulation of KiSS-1 mRNA expression by sex steroids in the brain of the male mouse. Endocrinology. 2005;146(7):2976-84.
26. Smith JT, Cunningham MJ, Rissman EF, Clifton DK, Steiner RA. Regulation of Kiss1 gene expression in the brain of the female mouse. Endocrinology. 2005;146(9):3686-92.
27. Pielecka-Fortuna J, Chu Z, Moenter SM. Kisspeptin acts directly and indirectly to increase gonadotropin-releasing hormone neuron activity and its effects are modulated by estradiol. Endocrinology. 2008;149(4):1979-86.
28. Richards JS, Russell DL, Robker RL, Dajee M, Alliston TN. Molecular mechanisms of ovulation and luteinization. Mol Cell Endocrinol. 1998;145(1-2):47-54.
29. Sealfon SC, Weinstein H, Millar RP. Molecular mechanisms of ligand interaction with the gonadotropin-releasing hormone receptor. Endocr Rev. 1997;18(2):180-205.
30. Blomenrohr M, Bogerd J, Leurs R, Goos H. Differences in structure-function relations between nonmammalian and mammalian GnRH receptors: what we have learnt from the African catfish GnRH receptor. Prog Brain Res. 2002;141:87-93.
31. Sun N, Kim KM. Mechanistic diversity involved in the desensitization of G protein-coupled receptors. Arch Pharm Res. 2021;44(4):342-53.
32. Hilger D, Masureel M, Kobilka BK. Structure and dynamics of GPCR signaling complexes. Nat Struct Mol Biol. 2018;25(1):4-12.
33. Magalhaes AC, Dunn H, Ferguson SS. Regulation of GPCR activity, trafficking and localization by GPCR-interacting proteins. Br J Pharmacol. 2012;165(6):1717-36.
34. Vrecl M, Heding A, Hanyaloglu A, Taylor PL, Eidne KA. Internalization kinetics of the gonadotropin-releasing hormone (GnRH) receptor. Pflugers Arch. 2000;439(Suppl 1):r019-r20.
35. Castro-Fernandez C, Conn PM. Regulation of the gonadotropin-releasing hormone receptor (GnRHR) by RGS proteins: role of the GnRHR carboxyl-terminus. Mol Cell Endocrinol. 2002;191(2):149-56.
36. Willars GB, Heding A, Vrecl M, Sellar R, Blomenrohr M, Nahorski SR, et al. Lack of a C-terminal tail in the mammalian gonadotropin-releasing hormone receptor confers resistance to

agonist-dependent phosphorylation and rapid desensitization. J Biol Chem. 1999;274(42):30146-53.
37. Davidson JS, Wakefield IK, Millar RP. Absence of rapid desensitization of the mouse gonadotropin-releasing hormone receptor. Biochem J. 1994;300 (Pt 2):299-302.
38. Perrett RM, McArdle CA. Molecular mechanisms of gonadotropin-releasing hormone signaling: integrating cyclic nucleotides into the network. Front Endocrinol (Lausanne). 2013;4:180.
39. Liu HK, Nestor KE, Long DW, Bacon WL. Frequency of luteinizing hormone surges and egg production rate in turkey hens. Biol Reprod. 2001;64(6):1769-75.
40. Williams BL, Akazome Y, Oka Y, Eisthen HL. Dynamic evolution of the GnRH receptor gene family in vertebrates. BMC Evol Biol. 2014;14:215.
41. Sefideh FA, Moon MJ, Yun S, Hong SI, Hwang JI, Seong JY. Local duplication of gonadotropin-releasing hormone (GnRH) receptor before two rounds of whole genome duplication and origin of the mammalian GnRH receptor. PLoS One. 2014;9(2):e87901.
42. Toufaily C, Schang G, Zhou X, Wartenberg P, Boehm U, Lydon JP, et al. Impaired LH surge amplitude in gonadotrope-specific progesterone receptor knockout mice. J Endocrinol. 2020;244(1):111-22.
43. Naor Z. Signaling by G-protein-coupled receptor (GPCR): studies on the GnRH receptor. Front Neuroendocrinol. 2009;30(1):10-29.
44. Oliva JL, Griner EM, Kazanietz MG. PKC isozymes and diacylglycerol-regulated proteins as effectors of growth factor receptors. Growth Factors. 2005;23(4):245-52.
45. Naor Z, Benard O, Seger R. Activation of MAPK cascades by G-protein-coupled receptors: the case of gonadotropin-releasing hormone receptor. Trends Endocrinol Metab. 2000;11(3):91-9.
46. Bliss SP, Miller A, Navratil AM, Xie J, McDonough SP, Fisher PJ, et al. ERK signaling in the pituitary is required for female but not male fertility. Mol Endocrinol. 2009;23(7):1092-101.
47. Yamada Y, Yamamoto H, Yonehara T, Kanasaki H, Nakanishi H, Miyamoto E, et al. Differential activation of the luteinizing hormone beta-subunit promoter by activin and gonadotropin-releasing hormone: a role for the mitogen-activated protein kinase signaling pathway in LbetaT2 gonadotrophs. Biol Reprod. 2004;70(1):236-43.
48. Harris D, Bonfil D, Chuderland D, Kraus S, Seger R, Naor Z. Activation of MAPK cascades by GnRH: ERK and Jun N-terminal kinase are involved in basal and GnRH-stimulated activity of the glycoprotein hormone LHbeta-subunit promoter. Endocrinology. 2002;143(3):1018-25.
49. Lariviere S, Garrel G, Simon V, Soh JW, Laverriere JN, Counis R, et al. Gonadotropin-releasing hormone couples to 3',5'-cyclic adenosine-5'-monophosphate pathway through novel protein kinase Cdelta and -epsilon in LbetaT2 gonadotrope cells. Endocrinology. 2007;148(3):1099-107.
50. Naor Z, Harris D, Shacham S. Mechanism of GnRH receptor signaling: combinatorial cross-talk of Ca2+ and protein kinase C. Front Neuroendocrinol. 1998;19(1):1-19.
51. Kwiecien R, Hammond C. Differential management of Ca2+ oscillations by anterior pituitary cells: a comparative overview. Neuroendocrinology. 1998;68(3):135-51.
52. McDowell IF, Morris JF, Charlton HM. Characterization of the pituitary gonadotroph cells of hypogonadal (hpg) male mice: comparison with normal mice. J Endocrinol. 1982;95(3):321-30.
53. McDowell IF, Morris JF, Charlton HM, Fink G. Effects of luteinizing hormone releasing hormone on the gonadotrophs of hypogonadal (hpg) mice. J Endocrinol. 1982;95(3):331-40.

54. Gibson MJ, Miller GM, Silverman AJ. Pulsatile luteinizing hormone secretion in normal female mice and in hypogonadal female mice with preoptic area implants. Endocrinology. 1991;128(2):965-71.
55. Pawson AJ, Faccenda E, Maudsley S, Lu ZL, Naor Z, Millar RP. Mammalian type I gonadotropin-releasing hormone receptors undergo slow, constitutive, agonist-independent internalization. Endocrinology. 2008;149(3):1415-22.
56. Griswold MD. The central role of Sertoli cells in spermatogenesis. Semin Cell Dev Biol. 1998;9(4):411-6.
57. Allan CM, Garcia A, Spaliviero J, Zhang FP, Jimenez M, Huhtaniemi I, et al. Complete Sertoli cell proliferation induced by follicle-stimulating hormone (FSH) independently of luteinizing hormone activity: evidence from genetic models of isolated FSH action. Endocrinology. 2004;145(4):1587-93.
58. Li Y, Schang G, Wang Y, Zhou X, Levasseur A, Boyer A, et al. Conditional Deletion of FOXL2 and SMAD4 in Gonadotropes of Adult Mice Causes Isolated FSH Deficiency. Endocrinology. 2018;159(7):2641-55.
59. Herbison AE, Porteous R, Pape JR, Mora JM, Hurst PR. Gonadotropin-releasing hormone neuron requirements for puberty, ovulation, and fertility. Endocrinology. 2008;149(2):597-604.
60. Czieselsky K, Prescott M, Porteous R, Campos P, Clarkson J, Steyn FJ, et al. Pulse and Surge Profiles of Luteinizing Hormone Secretion in the Mouse. Endocrinology. 2016;157(12):4794-802.
61. Heding A, Vrecl M, Hanyaloglu AC, Sellar R, Taylor PL, Eidne KA. The rat gonadotropin-releasing hormone receptor internalizes via a beta-arrestin-independent, but dynamin-dependent, pathway: addition of a carboxyl-terminal tail confers beta-arrestin dependency. Endocrinology. 2000;141(1):299-306.
62. Lin X, Janovick JA, Brothers S, Blomenrohr M, Bogerd J, Conn PM. Addition of catfish gonadotropin-releasing hormone (GnRH) receptor intracellular carboxyl-terminal tail to rat GnRH receptor alters receptor expression and regulation. Mol Endocrinol. 1998;12(2):161-71.
63. Cahill TJ, 3rd, Thomsen AR, Tarrasch JT, Plouffe B, Nguyen AH, Yang F, et al. Distinct conformations of GPCR-beta-arrestin complexes mediate desensitization, signaling, and endocytosis. Proc Natl Acad Sci U S A. 2017;114(10):2562-7.
64. Kumari P, Srivastava A, Ghosh E, Ranjan R, Dogra S, Yadav PN, et al. Core engagement with beta-arrestin is dispensable for agonist-induced vasopressin receptor endocytosis and ERK activation. Mol Biol Cell. 2017;28(8):1003-10.
65. Baidya M, Kumari P, Dwivedi-Agnihotri H, Pandey S, Sokrat B, Sposini S, et al. Genetically encoded intrabody sensors report the interaction and trafficking of beta-arrestin 1 upon activation of G-protein-coupled receptors. J Biol Chem. 2020;295(30):10153-67.
66. Dwivedi-Agnihotri H, Chaturvedi M, Baidya M, Stepniewski TM, Pandey S, Maharana J, et al. Distinct phosphorylation sites in a prototypical GPCR differently orchestrate beta-arrestin interaction, trafficking, and signaling. Sci Adv. 2020;6(37).
67. Owen CM, Zhou X, Bernard DJ, Jaffe LA. Kisspeptin-54 injection induces a physiological LH surge and ovulation in mice. Biol Reprod. 2021.
68. Lim S, Luo M, Koh M, Yang M, bin Abdul Kadir MN, Tan JH, et al. Distinct mechanisms involving diverse histone deacetylases repress expression of the two gonadotropin beta-subunit genes in immature gonadotropes, and their actions are overcome by gonadotropin-releasing hormone. Mol Cell Biol. 2007;27(11):4105-20.

69. Liu F, Ruiz MS, Austin DA, Webster NJ. Constitutively active Gq impairs gonadotropin-releasing hormone-induced intracellular signaling and luteinizing hormone secretion in LbetaT2 cells. Mol Endocrinol. 2005;19(8):2074-85.
70. Stutzin A, Stojilkovic SS, Catt KJ, Rojas E. Characteristics of two types of calcium channels in rat pituitary gonadotrophs. Am J Physiol. 1989;257(5 Pt 1):C865-74.
71. Perez-Reyes E, Yuan W, Wei X, Bers DM. Regulation of the cloned L-type cardiac calcium channel by cyclic-AMP-dependent protein kinase. FEBS Lett. 1994;342(2):119-23.
72. Berjukow S, Doring F, Froschmayr M, Grabner M, Glossmann H, Hering S. Endogenous calcium channels in human embryonic kidney (HEK293) cells. Br J Pharmacol. 1996;118(3):748-54.
73. Catt KJ, Stojilkovic SS. Calcium signaling and gonadotropin secretion. Trends Endocrinol Metab. 1989;1(1):15-20.
74. Tomic M, Cesnajaj M, Catt KJ, Stojilkovic SS. Developmental and physiological aspects of Ca2+ signaling in agonist-stimulated pituitary gonadotrophs. Endocrinology. 1994;135(5):1762-71.
75. Odle AK, Benes H, Melgar Castillo A, Akhter N, Syed M, Haney A, et al. Association of Gnrhr mRNA With the Stem Cell Determinant Musashi: A Mechanism for Leptin-Mediated Modulation of GnRHR Expression. Endocrinology. 2018;159(2):883-94.
76. Naik SI, Young LS, Saade G, Kujore A, Charlton HM, Clayton RN. Role of GnRH in the regulation of pituitary GnRH receptors in female mice. J Reprod Fertil. 1985;74(2):605-14.
77. Naik SI, Saade G, Detta A, Clayton RN. Homologous ligand regulation of gonadotrophin-releasing hormone receptors in vivo: relationship to gonadotrophin secretion and gonadal steroids. J Endocrinol. 1985;107(1):41-7.
78. Hochberg GKA, Thornton JW. Reconstructing Ancient Proteins to Understand the Causes of Structure and Function. Annu Rev Biophys. 2017;46:247-69.
79. Alarid ET, Windle JJ, Whyte DB, Mellon PL. Immortalization of pituitary cells at discrete stages of development by directed oncogenesis in transgenic mice. Development. 1996;122(10):3319-29.
80. Alvarez-Curto E, Inoue A, Jenkins L, Raihan SZ, Prihandoko R, Tobin AB, et al. Targeted Elimination of G Proteins and Arrestins Defines Their Specific Contributions to Both Intensity and Duration of G Protein-coupled Receptor Signaling. J Biol Chem. 2016;291(53):27147-59.
81. Finch AR, Sedgley KR, Caunt CJ, McArdle CA. Plasma membrane expression of GnRH receptors: regulation by antagonists in breast, prostate, and gonadotrope cell lines. J Endocrinol. 2008;196(2):353-67.
82. Namkung Y, Le Gouill C, Lukashova V, Kobayashi H, Hogue M, Khoury E, et al. Monitoring G protein-coupled receptor and beta-arrestin trafficking in live cells using enhanced bystander BRET. Nat Commun. 2016;7:12178.
83. Namkung Y, LeGouill C, Kumar S, Cao Y, Teixeira LB, Lukasheva V, et al. Functional selectivity profiling of the angiotensin II type 1 receptor using pathway-wide BRET signaling sensors. Sci Signal. 2018;11(559).
84. Khoury E, Nikolajev L, Simaan M, Namkung Y, Laporte SA. Differential regulation of endosomal GPCR/beta-arrestin complexes and trafficking by MAPK. J Biol Chem. 2014;289(34):23302-17.
85. Quoyer J, Janz JM, Luo J, Ren Y, Armando S, Lukashova V, et al. Pepducin targeting the C-X-C chemokine receptor type 4 acts as a biased agonist favoring activation of the inhibitory G protein. Proc Natl Acad Sci U S A. 2013;110(52):E5088-97.

86. Bardeesy N, Sinha M, Hezel AF, Signoretti S, Hathaway NA, Sharpless NE, et al. Loss of the Lkb1 tumour suppressor provokes intestinal polyposis but resistance to transformation. Nature. 2002;419(6903):162-7.
87. Farley FW, Soriano P, Steffen LS, Dymecki SM. Widespread recombinase expression using FLPeR (flipper) mice. Genesis. 2000;28(3-4):106-10.
88. Lakso M, Pichel JG, Gorman JR, Sauer B, Okamoto Y, Lee E, et al. Efficient in vivo manipulation of mouse genomic sequences at the zygote stage. Proc Natl Acad Sci U S A. 1996;93(12):5860-5.
89. Ongaro L, Schang G, Ho CC, Zhou X, Bernard DJ. TGF-beta Superfamily Regulation of Follicle-Stimulating Hormone Synthesis by Gonadotrope Cells: Is There a Role for Bone Morphogenetic Proteins? Endocrinology. 2019;160(3):675-83.
90. Li Y, Schang G, Wang Y, Zhou X, Levasseur A, Boyer A, et al. Conditional deletion of FOXL2 and SMAD4 in gonadotropes of adult mice causes isolated FSH deficiency. Endocrinology. 2018.
91. Schang G, Ongaro L, Schultz H, Wang Y, Zhou X, Brule E, et al. Murine FSH Production Depends on the Activin Type II Receptors ACVR2A and ACVR2B. Endocrinology. 2020;161(7).
92. Steyn FJ, Wan Y, Clarkson J, Veldhuis JD, Herbison AE, Chen C. Development of a methodology for and assessment of pulsatile luteinizing hormone secretion in juvenile and adult male mice. Endocrinology. 2013;154(12):4939-45.
93. Bernard DJ. Both SMAD2 and SMAD3 mediate activin-stimulated expression of the follicle-stimulating hormone beta subunit in mouse gonadotrope cells. Mol Endocrinol. 2004;18(3):606-23.
94. Livak KJ, Schmittgen TD. Analysis of relative gene expression data using real-time quantitative PCR and the 2(-Delta Delta C(T)) Method. Methods. 2001;25(4):402-8.
95. Namkung Y, Radresa O, Armando S, Devost D, Beautrait A, Le Gouill C, et al. Quantifying biased signaling in GPCRs using BRET-based biosensors. Methods. 2016;92:5-10.
96. Sleno R, Devost D, Petrin D, Zhang A, Bourque K, Shinjo Y, et al. Conformational biosensors reveal allosteric interactions between heterodimeric AT1 angiotensin and prostaglandin F2alpha receptors. J Biol Chem. 2017;292(29):12139-52.
97. Turgeon MO, Silander TL, Doycheva D, Liao XH, Rigden M, Ongaro L, et al. TRH Action Is Impaired in Pituitaries of Male IGSF1-Deficient Mice. Endocrinology. 2017;158(4):815-30.
98. Artimovich E, Jackson RK, Kilander MBC, Lin YC, Nestor MW. PeakCaller: an automated graphical interface for the quantification of intracellular calcium obtained by high-content screening. BMC Neurosci. 2017;18(1):72.

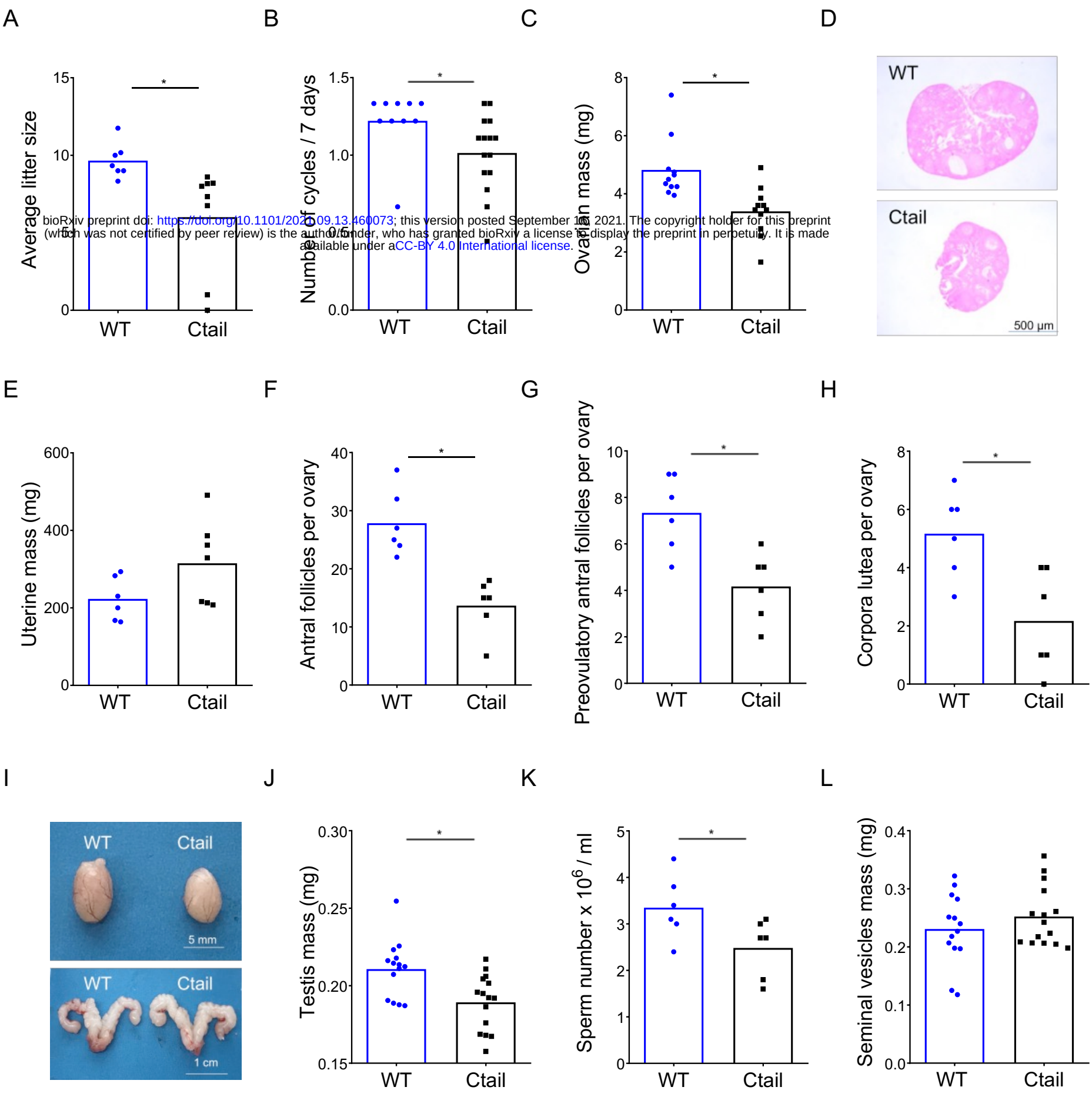

Figure 1: Ctail mice are hypogonadal and subfertile. (A) Average litter sizes in WT and Ctail females paired with WT C57BL/6 males over a six-month breeding trial (* p = 0.0196). (B) Estrous cycle frequency in WT and Ctail females (* p = 0.0384). (C) Ovarian mass of 10–12-week-old females (* p = 0.002). (D) H&E-stained ovarian sections from a WT and a Ctail mouse. (E) Uterine mass of 10–12-week-old females (ns, p = 0.088). Numbers of (F) antral follicles (* p = 0.0008), (G) preovulatory follicles (* p = 0.0055), and (H) corpora lutea per ovary (* p = 0.0088). (I) Testes (top) and seminal vesicles (bottom) from a WT and a Ctail male. (J) Testicular mass (* p = 0.0037), (K) number of mature spermatozoa per testis (* p = 0.0468), and (K) seminal vesicle mass (ns,p = 0.3123) in 10- to 12-week-old males. In A-C, E-H, and J-L, the bar height reflects the group mean and dots and squares reflect individual animals. Student *t*-tests were performed for statistical analysis.

Fig. 1

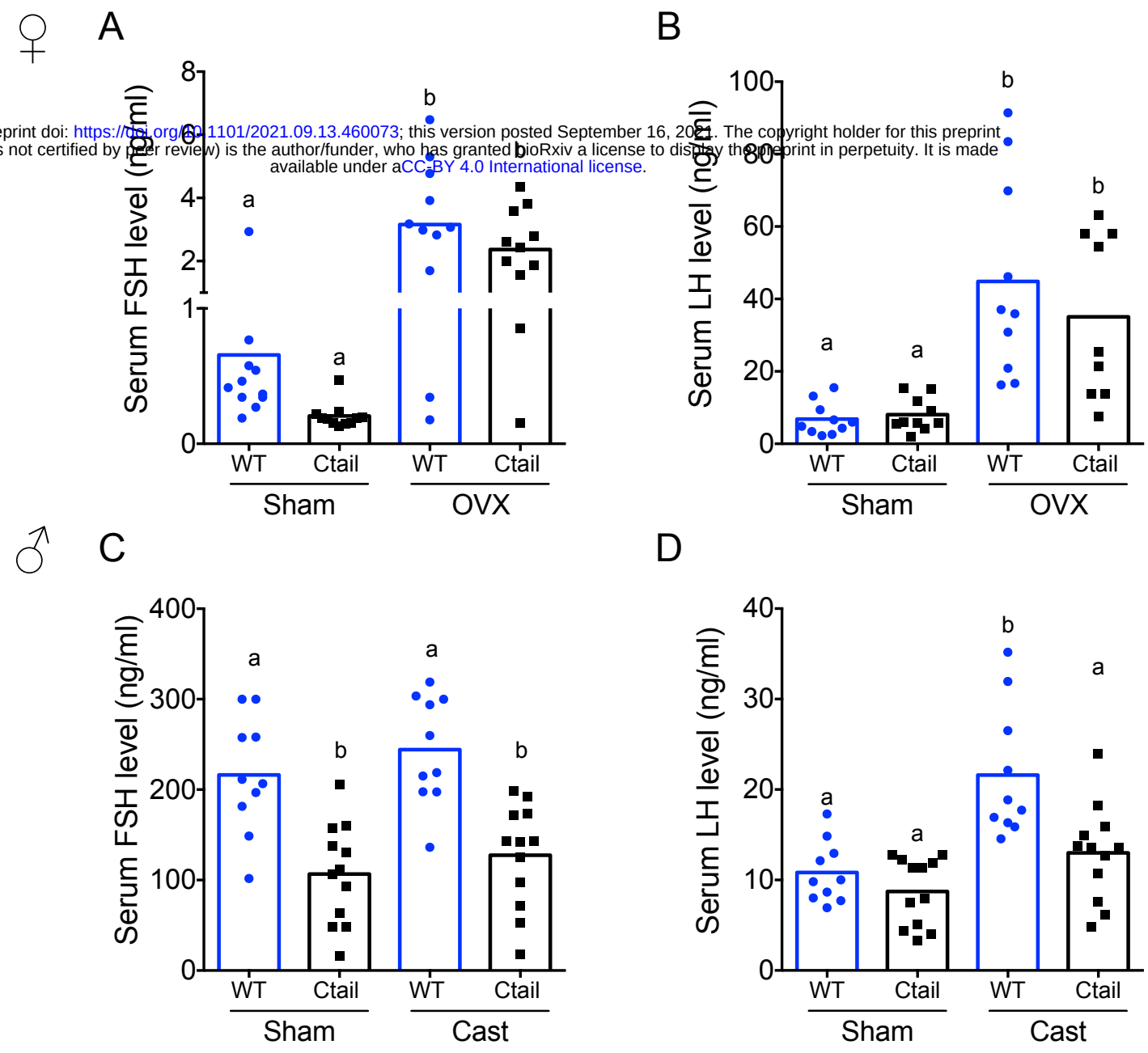

Figure 2: Serum FSH levels are reduced in Ctail mice. Serum (A, C) FSH and (B, D) LH levels were measured in 10- to 12-week-old sham-operated (Sham) or gonadectomized female (A, B) and male (C, D) WT and Ctail mice. Females were sampled on diestrus afternoon. Gonadectomized animals were sampled two-weeks post-ovariectomy (OVX) or castration (Cast). Male serum samples were measured with FSH/LH multiplex assays. In females, FSH was measured using an FSH Luminex assay and LH levels in females were measured by in-house ELISA. In each panel, the bar height reflects the group mean and dots and squares reflect individual animals. Statistical analyses in all panels were performed using two-way ANOVAs, followed by Tukey's multiple comparison tests. Bars with different letters differed significantly [Female FSH: WT (sham) vs. Ctail (sham) $p = 0.8241$; WT (sham) vs. WT (OVX) $p = 0.0001$; Ctail (sham) vs. Ctail (OVX) $p = 0.0010$; WT (OVX) vs. Ctail (OVX) $p = 0.4372$. Female LH: WT (sham) vs. Ctail (sham) $p = 0.99861$; WT (sham) vs. WT (OVX) $p = 0.0002$; Ctail (sham) vs. Ctail (OVX) $p = 0.0126$; WT (OVX) vs. Ctail (OVX) $p = 0.6399$; Male FSH: WT (sham) vs. Ctail (sham) $p = 0.0005$; WT (sham) vs. WT (Cast) $p = 0.7155$; Ctail (sham) vs. Ctail (Cast) $p = 0.8218$; WT (Cast) vs. Ctail (Cast) $p = 0.0002$. Male LH: WT (sham) vs. Ctail (sham) $p = 0.9162$; WT (sham) vs. WT (Cast) $p = 0.0002$; Ctail (sham) vs. Ctail (Cast) $p = 0.2477$; WT (Cast) vs. Ctail (Cast) $p = 0.0018$].

Fig. 2

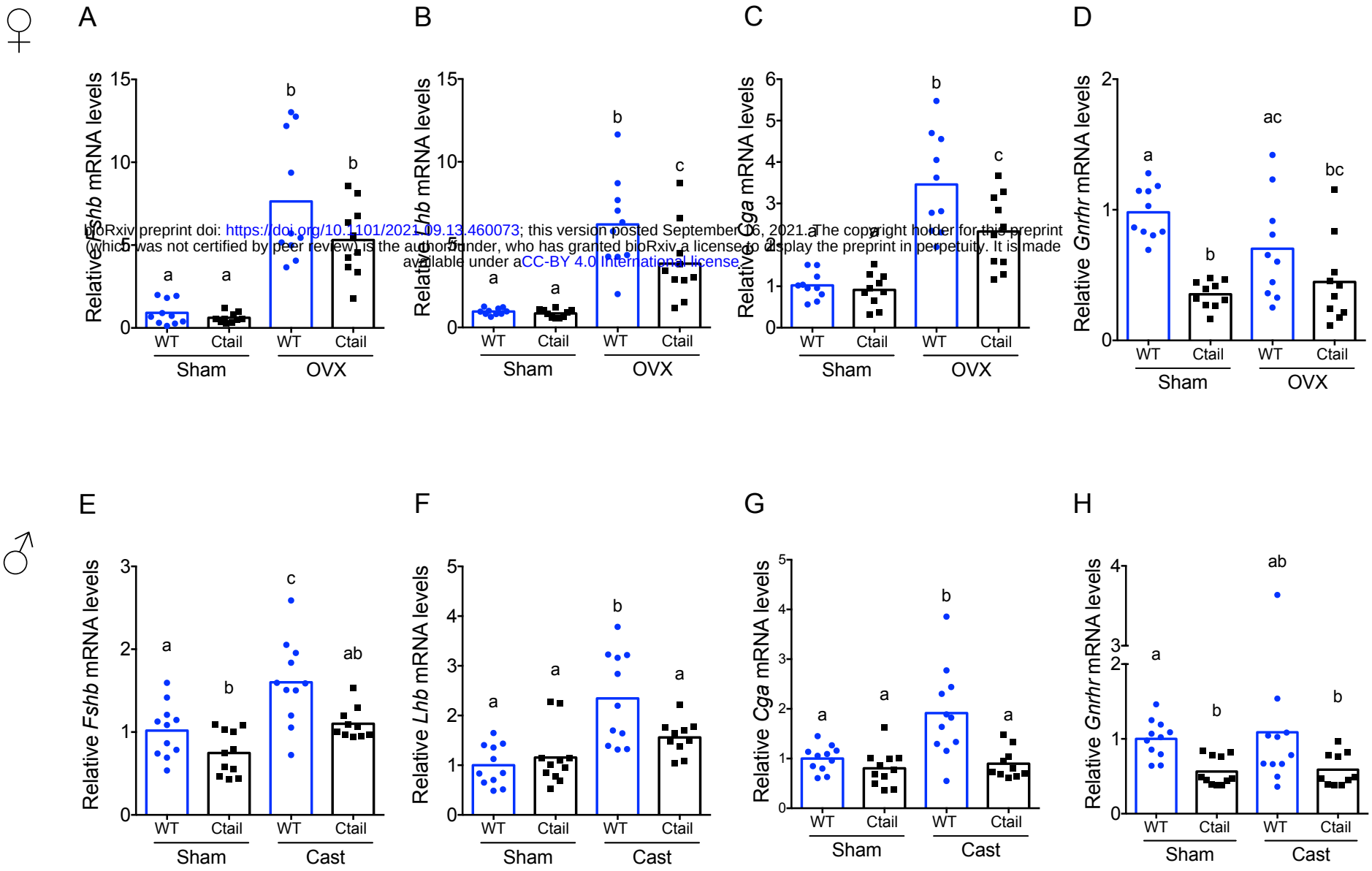

Figure 3: Pituitary gonadotropin subunit and *Gnrhr* mRNA levels were regulated by genotype and gonadal status. Relative pituitary (A, E) *Fshb*, (B, F) *Lhb*, (C, G) *Cga***,** and (D, H) *Gnrhr* mRNA levels in the mice from Figure 2 were measured by RT-qPCR. Gene expression was normalized to the reference gene ribosomal protein L19 (*Rpl19*). In each panel, the bar height reflects the group mean and dots and squares reflect individual animals. Statistical analyses were performed using two-way ANOVA tests, followed by Tukey's multiple comparison test. Bars with different letters differed significantly [Female *Fshb:* WT (sham) vs. Ctail (sham) $p = 0.99$; WT (sham) vs. WT (OVX) $p < 0.0001$; Ctail (sham) vs. Ctail (OVX) $p = 0.0002$; WT (OVX) vs. Ctail (OVX) $p = 0.1057$. Female *Lhb:* WT (sham) vs. Ctail (sham) $p = 0.9989$; WT (sham) vs. WT (OVX) $p < 0.0001$; Ctail (sham) vs. Ctail (OVX) $p = 0.0033$; WT (OVX) vs. Ctail (OVX) $p = 0.0267$. Female *Cga*: WT (sham) vs. Ctail (sham) $p = 0.9893$; WT (sham) vs. WT (OVX) $p < 0.0001$; Ctail (sham) vs. Ctail (OVX) $p = 0.0016$; WT (OVX) vs. Ctail (OVX) $p = 0.0138$. Female *Gnrhr*: WT (sham) vs. Ctail (sham) $p < 0.0001$; WT (sham) vs. WT (OVX) $p = 0.1332$; Ctail (sham) vs. Ctail (OVX) $p = 0.8731$; WT (OVX) vs. Ctail (OVX) $p = 0.1922$. Male *Fshb*: WT (sham) vs. Ctail (sham) $p = 0.0468$; WT (sham) vs. WT (Cast) $p = 0.0019$; Ctail (sham) vs. Ctail (Cast) $p = 0.1103$; WT (Cast) vs. Ctail (Cast) $p = 0.0109$. Male *Lhb*: WT (sham) vs. Ctail (sham) $p = 0.9345$; WT (sham) vs. WT (Cast) $p < 0.0001$; Ctail (sham) vs. Ctail (Cast) $p = 0.4394$; WT (Cast) vs. Ctail (Cast) $p = 0.0266$. Male *Cga*: WT (sham) vs. Ctail (sham) $p = 0.8192$; WT (sham) vs. WT (Cast) $p = 0.0013$; Ctail (sham) vs. Ctail (Cast) $p = 0.9772$; WT (Cast) vs. Ctail (Cast) $p = 0.0005$. Male *Gnrhr*: WT (sham) vs. Ctail (sham) $p = 0.0029$; WT (sham) vs. WT (Cast) $p = 0.6634$; Ctail (sham) vs. Ctail (Cast) $p > 0.9999$; WT (Cast) vs. Ctail (Cast) $p = 0.5638$].

Fig. 3

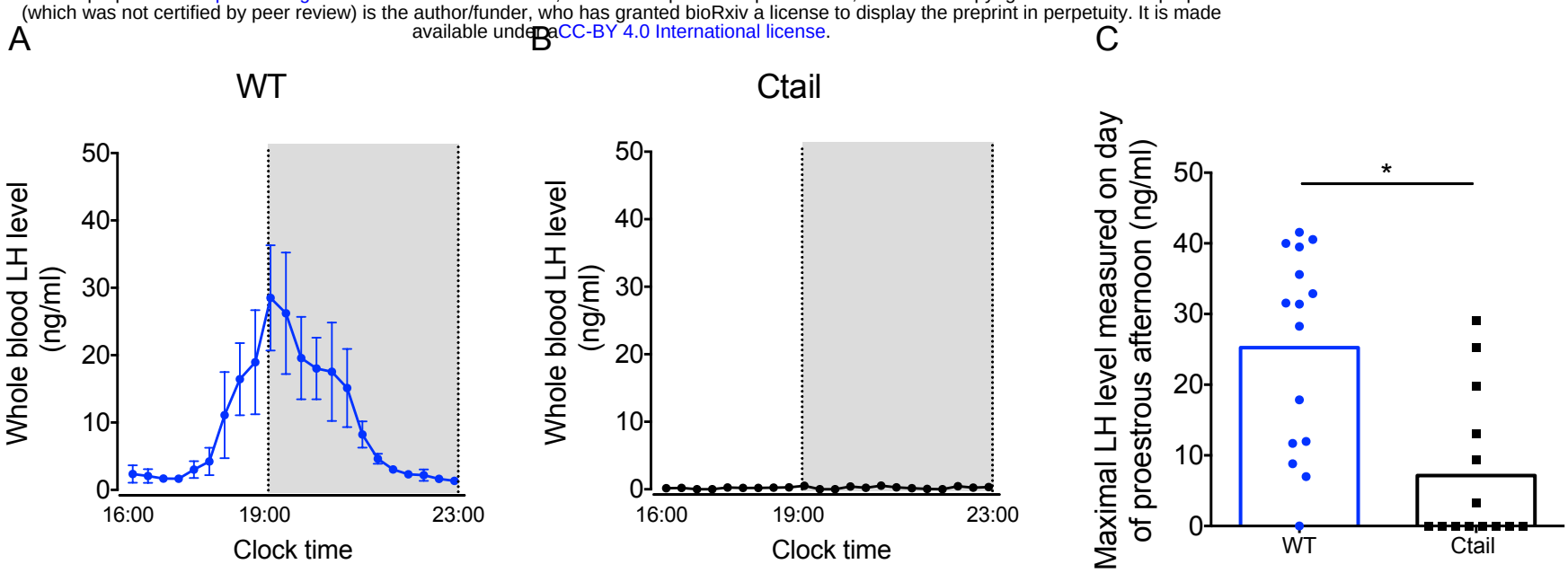

Figure 4: LH surge amplitude is attenuated in Ctail females. (A) Preovulatory LH surge profiles in WT (N = 5) and (B) Ctail females (N = 5) on proestrus, as identified by vaginal cytology. Blood samples were collected every 20 minutes from 4:00 PM (16:00) to 11:00 PM (23:00). Gray areas represent the dark phase of the light/dark cycle. (C) Maximal LH levels measured on proestrus from WT and Ctail females sampled 4 times daily for 11 days (see *Methods*). LH levels were measured in whole blood by with an in-house ELISA. In panels A and B, each dot reflects the group mean ± SEM. In C, the bar height reflects the group mean and dots and squares reflect individual animals. A Student *t*-test was performed for statistical analysis, * p = 0.0006.

Fig. 4

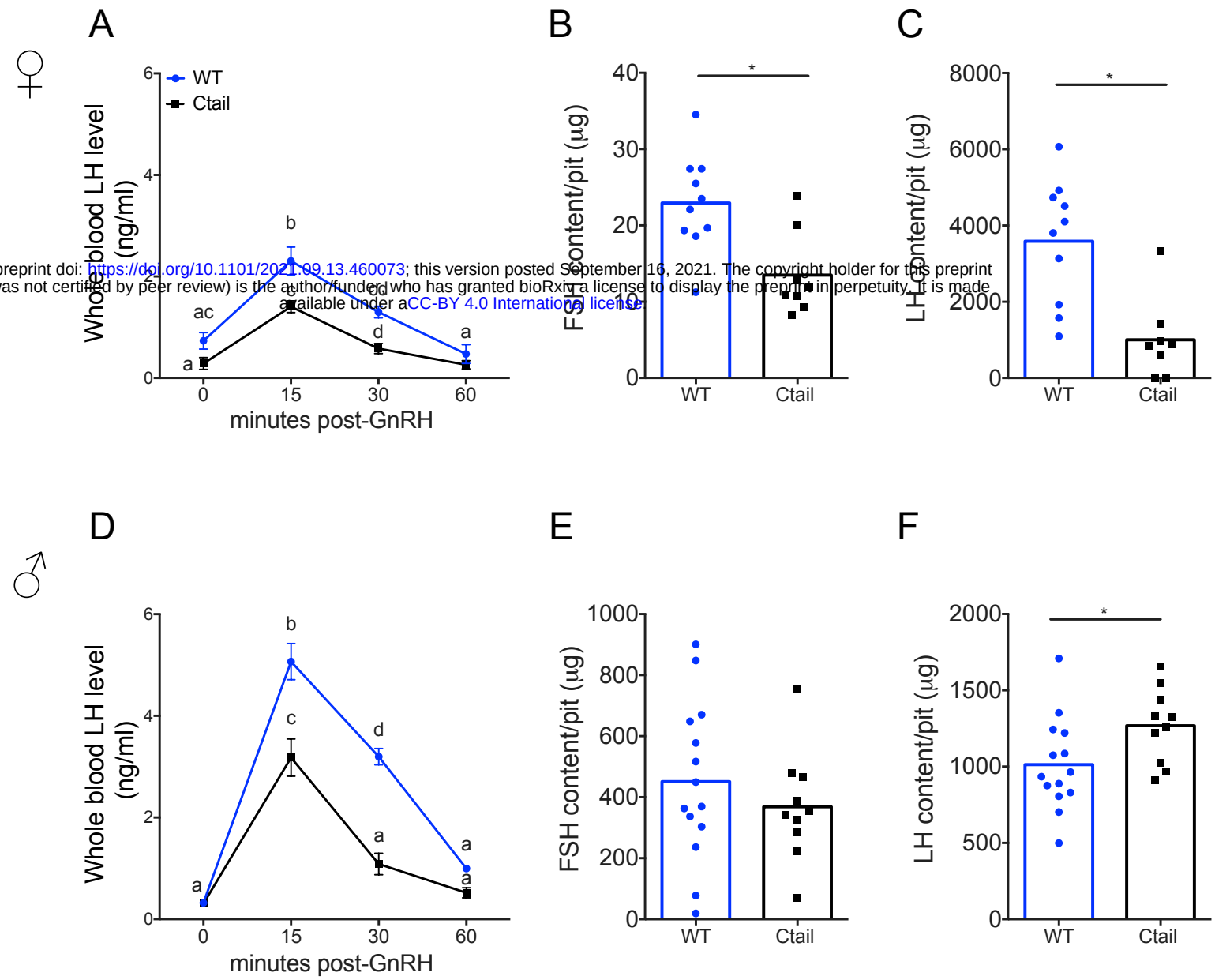

Figure 5: GnRH-stimulated LH release is attenuated in Ctail mice. Whole blood LH levels in 10–12-week-old (A) female and (D) male WT (blue, N = 12 females and N = 14 males) and Ctail (black, N = 9 for females and N = 11 for males) mice before (0) and 15-, 30-, and 60-min post i.p. injection of 1.25 ng of GnRH per g of body mass. Each point is the mean ± SEM. Data were analyzed using two-way ANOVAs, followed by Tukey's post-hoc tests for multiple comparisons. Points with different letters differ significantly (females WT vs. Ctail: 0 min $p = 0.0514$; 15 min $p = 0.0139$; 30 min $p = 0.0002$, 60 min $p = 0.3536$; males WT vs. Ctail: 0 min $p = 0.959653$; 15 min $p < 0.0001$; 30 min $p < 0.0001$, 60 min $p = 0.1112$). Intrapituitary contents of (B,E) FSH and (C,F) LH in randomly-cycling (B,C) female and (E,F) male WT and Ctail mice. The bar height reflects the group mean and dots and squares reflect individual animals. Data were analyzed by Student *t*-tests [B, * $p = 0.0043$; C, *$p = 0.0122$; E, * $p = 0.3977$; F, * $p = 0.0394$]. FSH levels were measured using a Luminex assay in females and by RIA in males. LH levels were measured with the in-house ELISA in both sexes.

Fig. 5

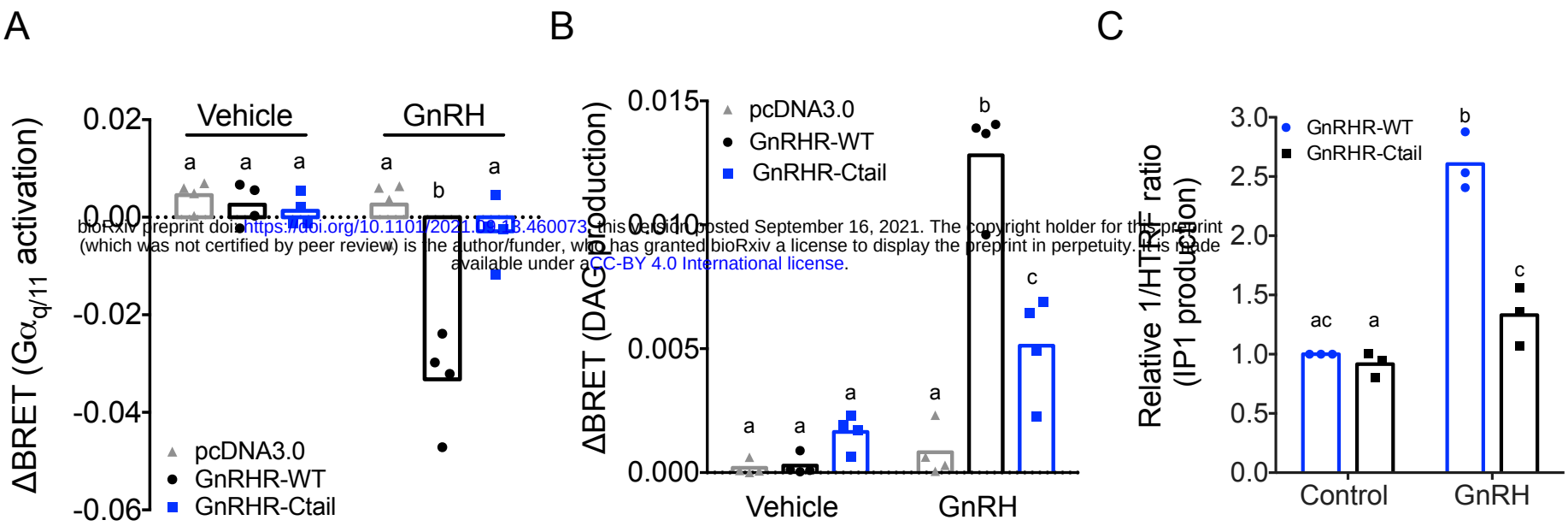

Figure 6: GnRH activation of G_q, diacylglycerol, and inositol phosphate via GnRHR-Ctail is impaired in heterologous cells. HEK 293 cells were transfected with empty vector (pcDNA3.0), GnRH-WT, or GnRHR-Ctail with (A) G_q or (B) DAG BRET-based biosensors. Cells were loaded with Coelenterazine 400a for 5 min, and luminescence values recorded 10 sec before and 30 sec post-treatment with vehicle (water) or 100 nM GnRH. ΔBRET values were calculated as the average of BRET values before treatment minus the average values post-treatment. Data are shown from 4 independent experiments. Bar heights reflect group means. (C) HEK 293 cells were transfected with GnRHR-WT or GnRHR-Ctail. Cells were treated with vehicle or 100 nM GnRH for 30 min. IP1 production was measured and reported as represented as the inverse of the Homogeneous Time Resolved Fluorescence (HTRF) ratio relative to control condition. Data are shown from 3 independent experiments. Bar heights reflect group means. In all panels, two-way ANOVAs followed by Tukey's multiple comparison test was used for statistical analysis. Different letters indicate statistically significant differences. In (A), untreated vs. treated with GnRH: pcDNA3.0 $p = 0.9969$; GnRHR-WT $p < 0.0001$ and GnRHR-Ctail $p = 0.9093$. In GnRH treated conditions: pcDNA3.0 vs GnRHR-WT $p < 0.0001$; pcDNA3.0 vs. GnRHR-Ctail $p = 0.7775$, and GnRHR-WT vs. GnRHR-Ctail $p < 0.000$, and in (B), untreated vs. treated with GnRH: pcDNA3.0 $p = 0.9838$; GnRHR-WT $p < 0.0001$ and GnRHR-Ctail $p = 0.0180$. In GnRH treated conditions: pcDNA3.0 vs GnRHR-WT $p < 0.0001$; pcDNA3.0 vs. GnRHR-Ctail $p = 0.0029$, and GnRHR-WT vs. GnRHR-Ctail $p < 0.0001$. In (C), GnRHR-WT (control) vs. GnRHR-Ctail (control) $p = 0.6321$; GnRHR-WT (control) vs. GnRHR-WT (GnRH) $p = 0.0004$; GnRHR-Ctail (control) vs. GnRHR-Ctail (GnRH) $p = 0.0170$; GnRHR-WT (GnRH) vs. GnRHR-Ctail (GnRH) $p = 0.0073$).

Fig. 6

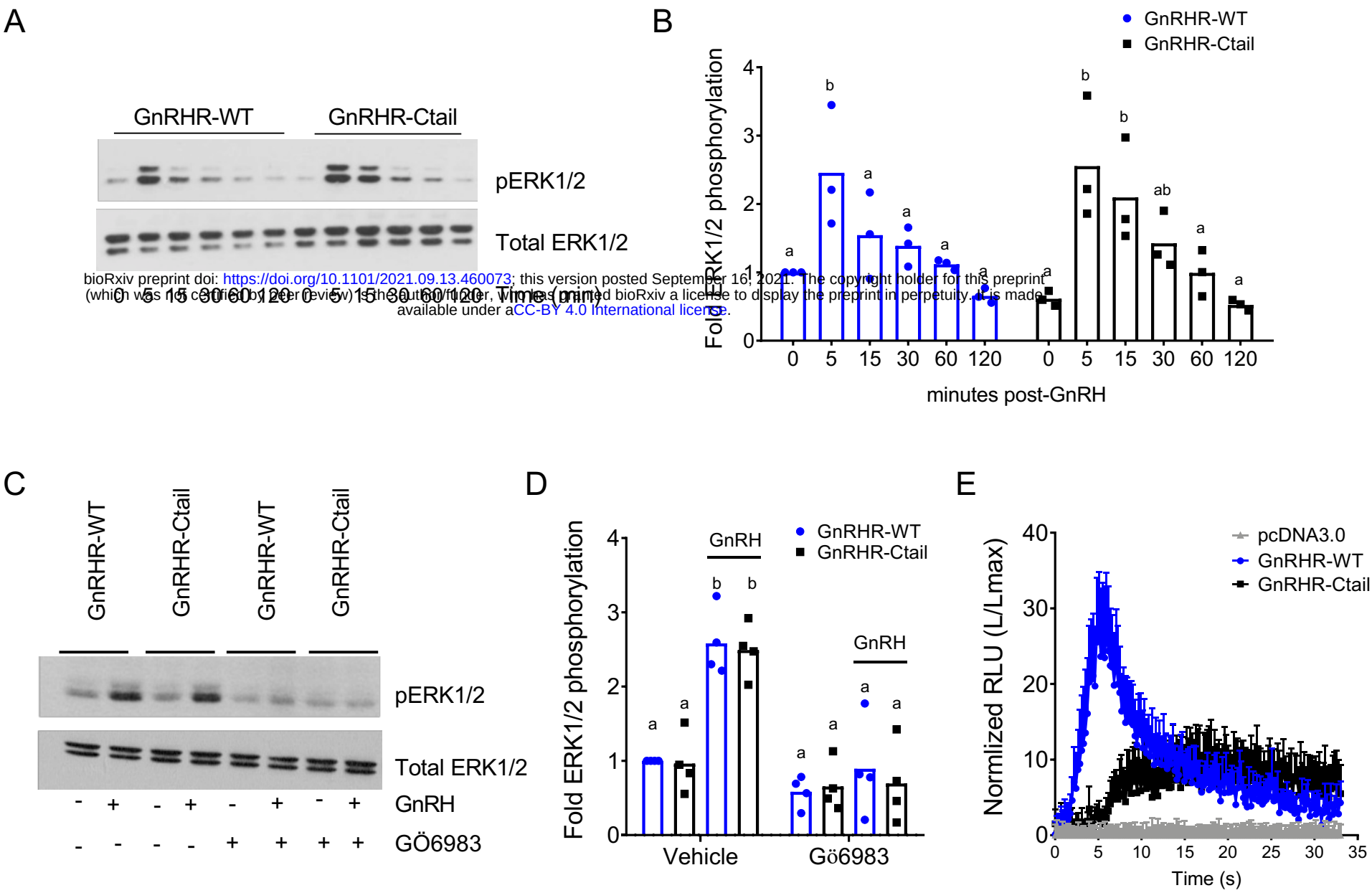

Figure 7: GnRH-stimulated intracellular calcium mobilization, but not ERK1/2 phosphorylation, is attenuated via GnRH-Ctail in heterologous cells. (A) HEK 293 cells were transfected with GnRH-WT or GnRHR-Ctail. Twenty-four hours post-transfection, cells were treated with vehicle (water; 0) as control or 100 nM GnRH for 5, 15, 30, 60 and 120 minutes. Whole cell protein lysates were collected and subjected to SDS-PAGE and western blotting with phospho- (top) or total (bottom) ERK1/2 antibodies. Blots from 1 of 3 replicate experiments are shown. (B) Data from the 3 independent experiments exemplified in panel A were quantified by normalizing the densitometry for pERK1/2 to total ERK1/2 and are presented relative to the control condition of the WT receptor. Two-way ANOVA followed by Tukey's multiple comparison test was used for statistical analysis. Bars with different letters differed significantly. GnRH-WT: 0 vs. 5 min $p = 0.0179$; 0 vs. 15 min $p = 0.7673$; 0 vs. 30 min $p = 0.9309$; 0 vs. 120 min $p = 0.9572$; GnRH-Ctail: 0 vs. 5 min $p = 0.0010$; 0 vs. 15 min $p = 0.0156$; 0 vs. 30 min $p = 0.3846$; 0 vs.120 min $p > 0.9999$). (C) HEK 293 cells were transfected with GnRH-WT or GnRHR-Ctail. Twenty-four h post-transfection, cells were pretreated with 5 μM pan-PKC inhibitor GÖ6983 for 20 min, and then treated with vehicle (water) or 100 nM GnRH for 5 min. Western blotting was performed as in panel A. One blot from 4 independent experiments is presented. (D) Data from the 4 independent experiments exemplified in panel C were quantified and statistically analyzed as in panel B. In GnRH treated conditions: GnRHR-WT (vehicle) vs. GnRHR-Ctail (vehicle) $p > 0.9999$; GnRHR-WT (Gö6983) vs. GnRHR-Ctail (Gö6983) $p = 0.9969$; GnRHR-WT (vehicle) vs. GnRHR-WT (Gö6983) $p = 0.0001$; GnRHR-Ctail (vehicle) vs. GnRHR-Ctail (Gö6983) $p < 0.0001$. (E) HEK 293 cells were transfected with GnRHR-WT, GnRHR-Ctail or empty vector (pcDNA3.0) along with the luminescence Obelin biosensor. Twenty-four h post-transfection, cells were loaded with Coelenterazine cp for 2 h. Cells were then treated with 100 nM GnRH. Intracellular Ca^{2+} was measured as relative luminescence emitted every 22 ms over 0.5 min. Data are presented as the ratio of total luminescence after GnRH over maximal luminescence (not shown) following Triton X-100 treatment from 3 independent experiments (mean ± SEM).

Fig. 7

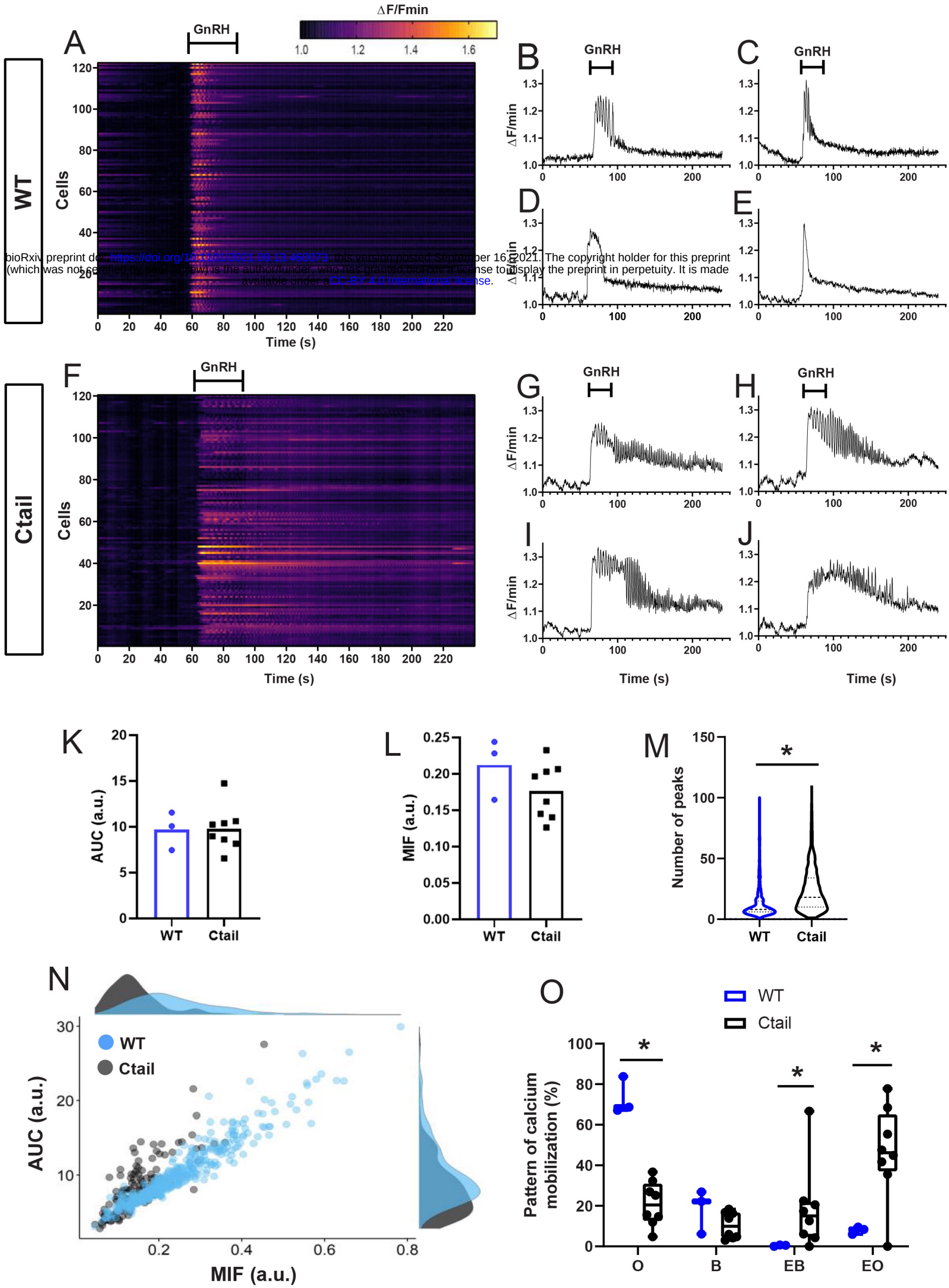

Fig. 8

Figure 8: GnRH-stimulated calcium responses are altered in gonadotropes of Ctail mice. Raster plots of calcium responses in gonadotropes from a representative adult male (A) WT and (F) Ctail mouse. Each row represents an individual cell. Cells are numbered on the y-axis. The x-axis shows time in seconds. The timing of GnRH administration is indicated. The heat map at the top shows the strength of the response, with yellower colors reflecting stronger calcium responses. Examples of calcium responses in individual gonadotropes from (B-E) wild-type and (G-J) Ctail mice. (K) Area under the curve (AUC) and (L) maximum intensity of fluorescence (MIF) were quantified (N = 3 WT and N = 8 Ctail). (M) Numbers of oscillatory peaks were also quantified [$p < 0.0001$; N = 3 (710 cells) WT and N = 8 (534 cells) Ctail]. (N) Correlation between AUC vs. MIF measurements from one mouse per genotype (250 cells of WT and 128 cells of Ctail). (O) Comparison of the calcium pattern of response (N = 3 WT and N = 8 Ctail): Oscillatory (O), (73.223 ± 7.489 vs 21.037 ± 10.262; WT vs Ctail, respectively, p = 0.0121); biphasic (B) (18.388 ± 8.885 vs 10.430 ± 6.075; WT vs Ctail, respectively, p = ns); extended biphasic (EB) (0.419 ± 0.307 vs 21.444 ± 19.528; WT vs Ctail, respectively, p = 0.0167); and extended oscillatory (EO) (7.969 ± 1.497 vs 53.036 ± 14.069; WT vs Ctail, respectively, p = 0.0167). Statistical analyses were performed using Wilcoxon rank-sum tests.

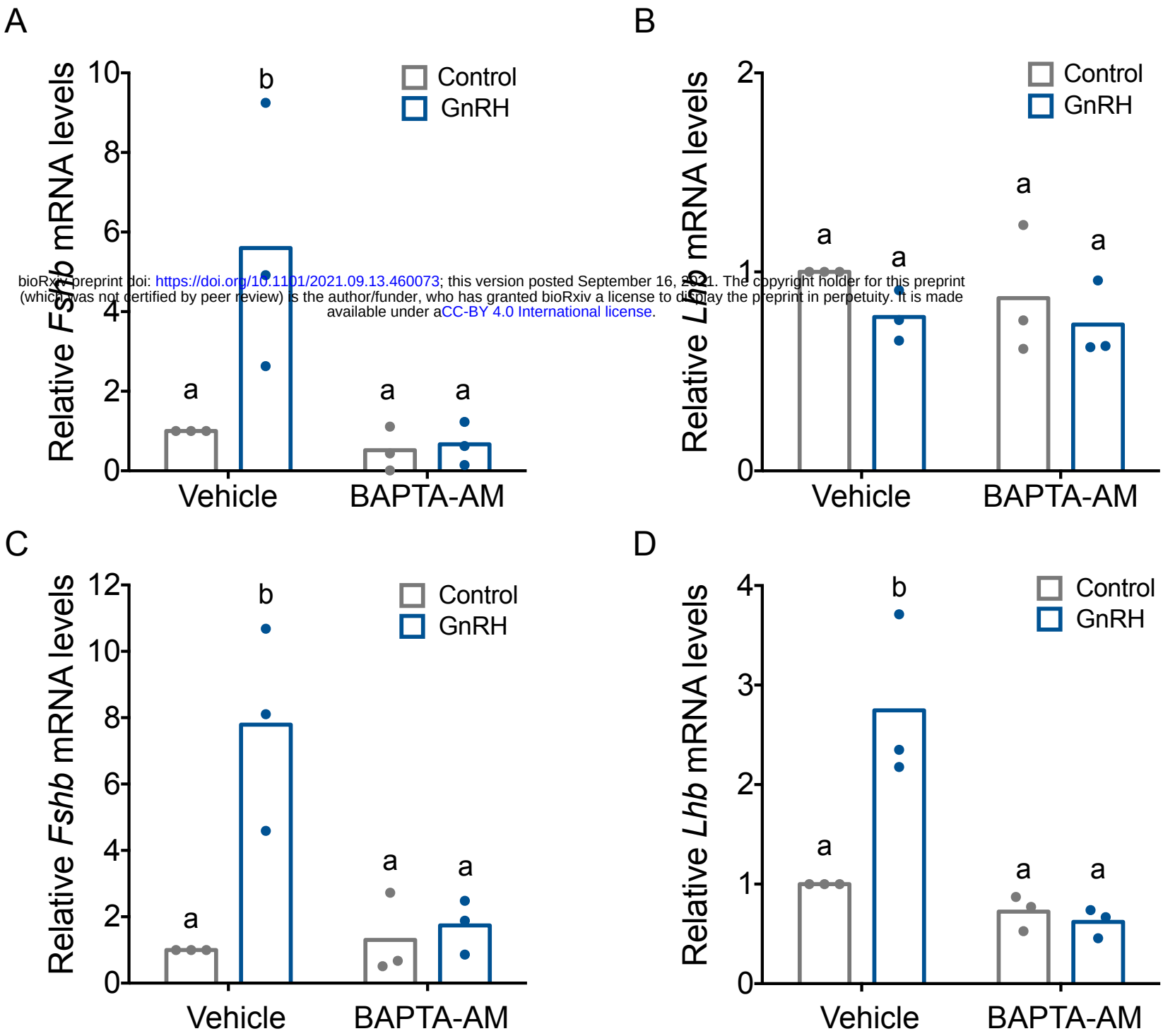

Figure 9: GnRH-induced *Fshb* expression is calcium-dependent in homologous LβT2 cells. Relative *Fshb* (A-C) and *Lhb* (B-D) expression in LβT2 cells treated with vehicle (DMSO) or 20 μM BAPTA-AM for 20 min followed by treatment with water (control) or low (A, B) or high GnRH (10 nM) pulse frequency (C, D). Gene expression was assessed by RT-qPCR and normalized to the reference gene ribosomal protein L19 (*Rpl19*). Data shown are from 3 independent experiments. The bar heights reflect group means. Data were analyzed with two-way ANOVAs, followed by post-hoc Tukey test for multiple comparisons. Bars with different letters differed significantly. Panel A: control (vehicle) vs. GnRH (vehicle) $p = 0.0193$; control (vehicle) vs. control (BAPTA-AM) $p = 0.9981$; control (vehicle) vs. GnRH (BAPTA-AM) $p = 0.9933$; GnRH (vehicle) vs. GnRH (BAPTA-AM) $p = 0.0122$]. Panel B: control (vehicle) vs. GnRH (vehicle) $p = 0.5389$; control (vehicle) vs. control (BAPTA-AM) $p = 0.8495$; control (vehicle) vs. GnRH (BAPTA-AM) $p = 0.4184$; GnRH (vehicle) vs. GnRH (BAPTA-AM) $p = 0.9951$. Panel C: control (vehicle) vs. GnRH (vehicle) $p = 0.0072$; control (vehicle) vs. control (BAPTA-AM) $p > 0.9999$; control (vehicle) vs. GnRH (BAPTA-AM) $p = 0.9964$; GnRH (vehicle) vs. GnRH (BAPTA-AM) $p = 0.0143$. Panel D: control (vehicle) vs. GnRH (vehicle) $p = 0.0052$; control (vehicle) vs. control (BAPTA-AM) $p = 0.8627$; control (vehicle) vs. GnRH (BAPTA-AM) $p = 0.7190$; GnRH (vehicle) vs. GnRH (BAPTA-AM) $p = 0.0015$.

Fig. 9

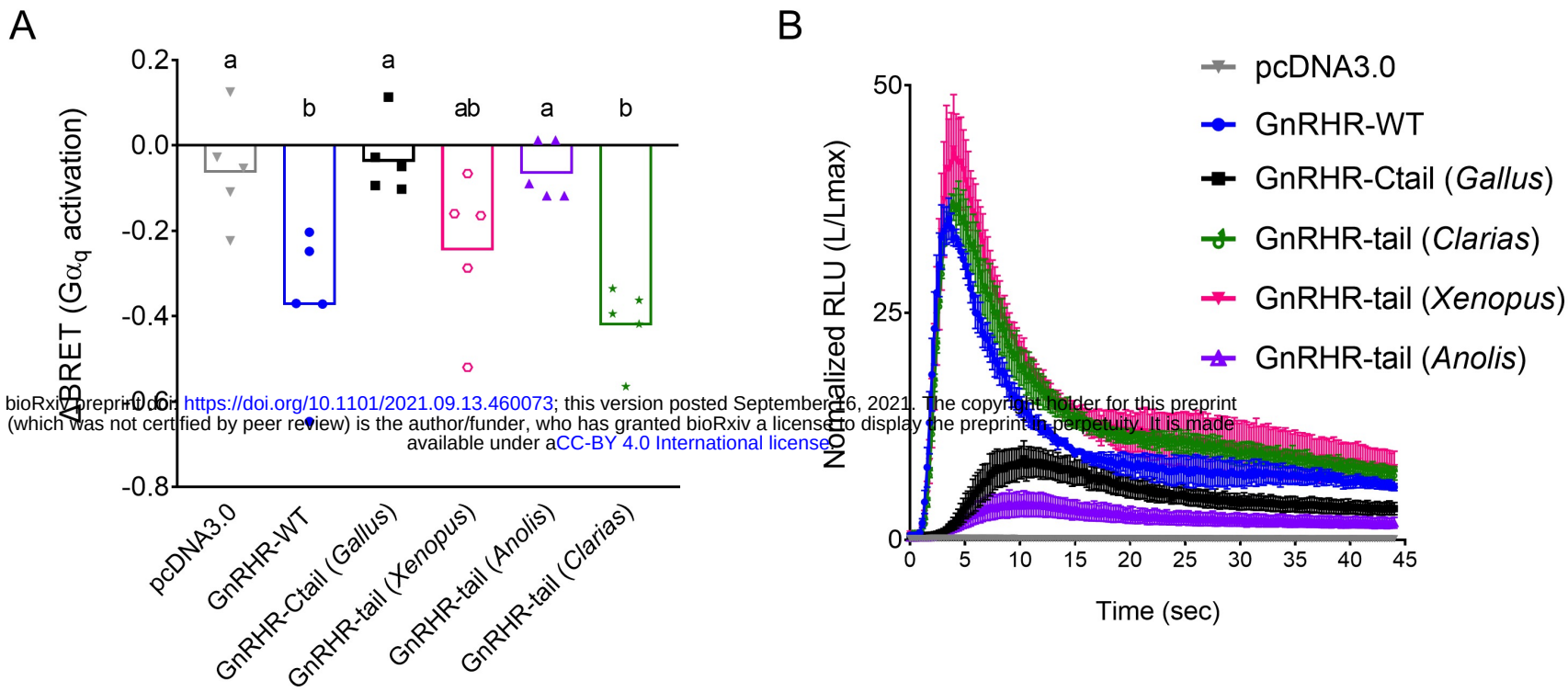

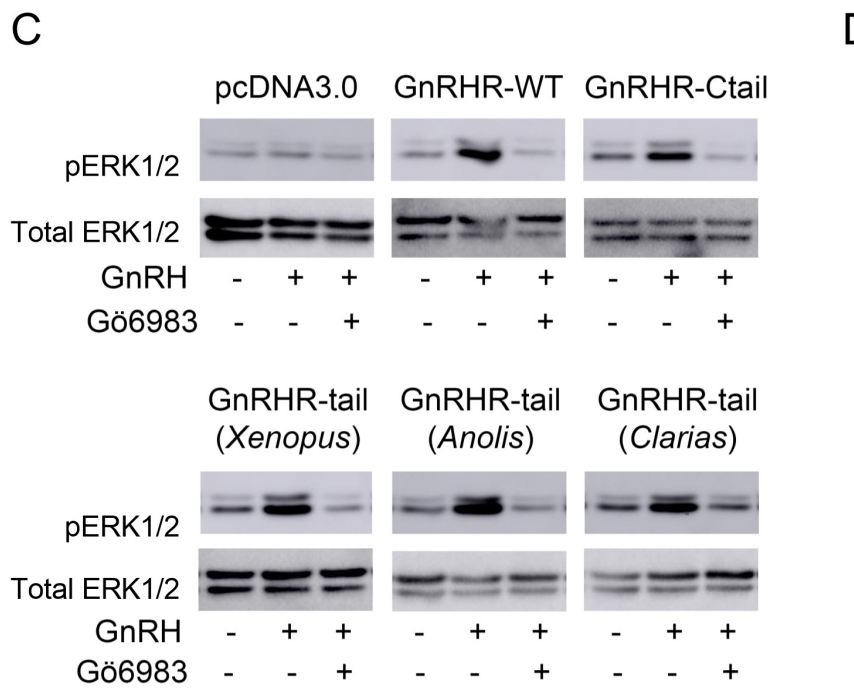

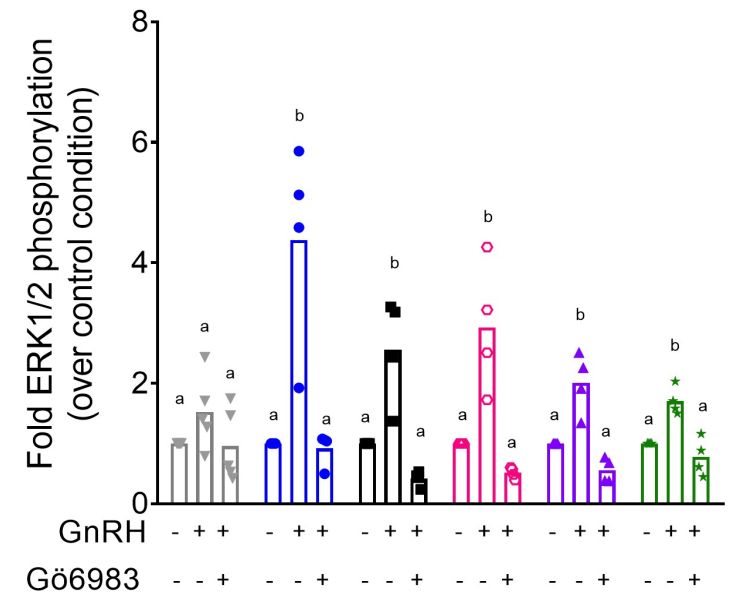

Figure 10: Disruption of GnRH signaling via chimeric GnRHRs depends on the sequence of the C-tail. (A) HEK 293 cells were transfected with the G_q biosensor and expression vectors for the indicated chimeric GnRHRs. Cells were treated with GnRH as in Figure 6A. BRET signals were read 3 times before and after GnRH stimulation. ΔBRET values are as described in Figure 6. Data are shown from 5 independent experiments. Bars heights reflect the group means. Data were analyzed with one-way ANOVAs, followed by post-hoc Tukey test for multiple comparisons. Different letters differed significantly. pcDNA3.0 vs. GnRHR-WT p = 0.0086; pcDNA3.0 vs. GnRHR-Ctail p = 0.9995; pcDNA3.0 vs GnRHR-tail (*Xenopus*) p = 0.2477; pcDNA3.0 vs. GnRHR-tail (*Anolis*) p > 0.9999; pcDNA3.0 vs. GnRHR-tail (*Clarias*) p = 0.0021. (B) HEK 293 cells were transfected with the luminescence Obelin biosensor and expression vectors for the indicated chimeric GnRHRs. Cells were treated with GnRH and analyzed as in Figure 7E. The mean ± SEM of 4 independent experiments is shown. (C) HEK 293 cells were transfected with the expression vectors for the indicated chimeric GnRHRs and treated and analyzed as in Figure 7C. The western blot shown is representative of 4 independent experiments. (D) The data exemplified in panel C were quantified and analyzed as in Figure 7B. Bar heights reflect group means. Data were analyzed with one-way ANOVA, for each receptor, followed by post-hoc Tukey test for multiple comparisons. Bars with different letters differed significantly. pcDNA3.0: control (vehicle) vs. GnRH (vehicle) p = 0.4955; GnRH (vehicle) vs. GnRH (Gö6983) p = 0.1373. GnRHR-WT: control (vehicle) vs. GnRH (vehicle) p = 0.0027; GnRH (vehicle) vs. GnRH (Gö6983) p = 0.0023. GnRHR-Ctail: control (vehicle) vs. GnRH (vehicle) p = 0.0050; GnRH (vehicle) vs. GnRH (Gö6983) p = 0.0006. GnRHR-tail (*Xenopus*): control (vehicle) vs. GnRH (vehicle) p = 0.0046; GnRH (vehicle) vs. GnRH (Gö6983) p = 0.0010. GnRHR-tail (*Anolis*): control (vehicle) vs. GnRH (vehicle) p = 0.0036; GnRH (vehicle) vs. GnRH (Gö6983) p = 0.0003. GnRHR-tail (*Clarias*): control (vehicle) vs. GnRH (vehicle) p = 0.0043; GnRH (vehicle) vs. GnRH (Gö6983) p = 0.0007.

Fig. 10

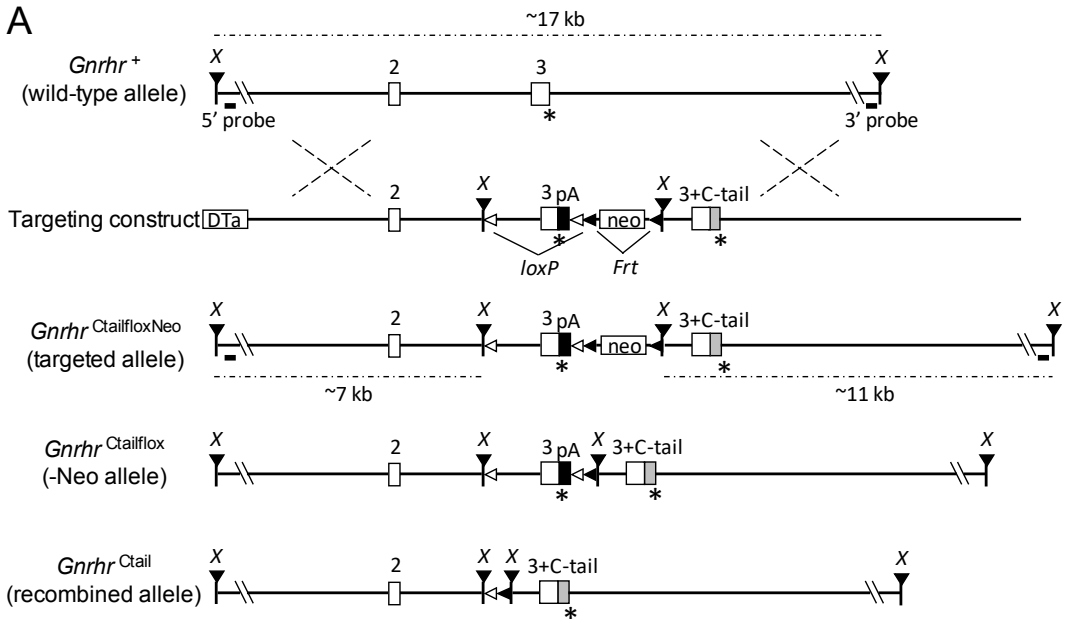

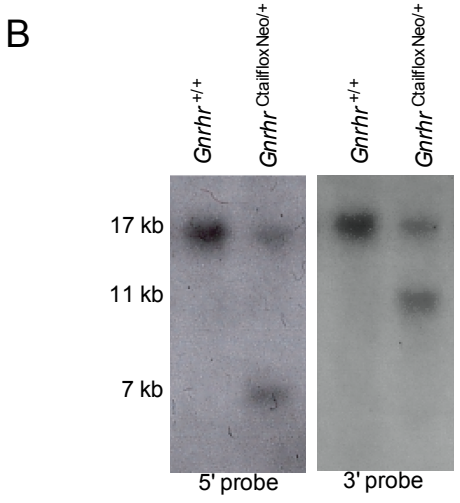

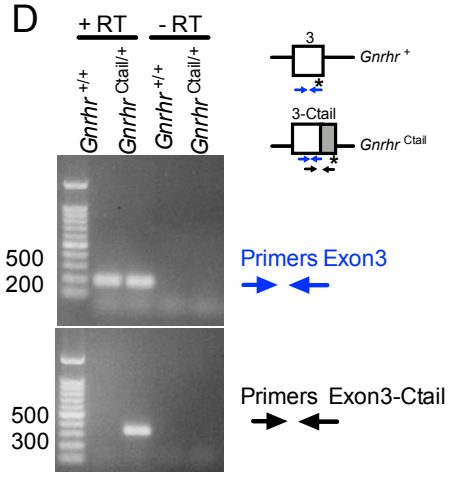

C

Genotype	*Gnrhr* $^{+/+}$	*Gnrhr* $^{Ctail/+}$	*Gnrhr* $^{Ctail/Ctail}$
Number	37	75	36
Expected %	25 %	50 %	25 %
Observed %	25 %	50.7 %	24.3 %

Figure 1-figure supplement 1

Figure 1-figure supplement 1: Generation of Ctail mice by gene targeting in embryonic stem cells. (A) Targeting strategy showing the wild-type *Gnrhr* allele (*Gnrhr*$^{+}$), the targeting construct, the targeted allele (*Gnrhr*^{CtailfloxNeo}), the Flp-recombined allele (*Gnrhr*^{Ctailflox}; -Neo), and the Cre recombined allele (*Gnrhr*^{Ctail}). Exons 2 and 3 are shown as white boxes, with their corresponding numbers above. The asterisks (*) indicate STOP codons. "*X*" refers to *Xma*I restriction sites. The positions of the 5' and 3' Southern blot probes are shown as horizontal lines below the wild-type and targeted alleles. The sizes of the *Xma*I restriction fragments, detected by the 5' and 3' Southern blot probes, are indicated above the wild-type and below the targeted alleles. The *loxP* sites are indicated with open triangles, and the *Frt* sites with black (leftward facing) triangles. The chimeric murine exon 3 fused to the coding sequence of the chicken GnRHR C-tail (indicated by a grey box) is the labelled as exon "3+C-tail". pA: bovine growth hormone polyA signal sequence; Neo: neomycin resistance cassette; DTa: diphtheria toxin A chain negative selection marker. (B) Confirmation of successful gene targeting and germline transmission of the modified allele. Southern blot with 5' (left) and 3' probes (right) performed on genomic DNA from a WT (*Gnrhr*$^{+/+}$) and a heterozygous mouse carrying the targeted allele (*Gnrhr*$^{CtaifloxNeo/+}$). (C) Ctail mice were born at the expected frequency. Number and percentage (%) of WT (*Gnrhr*$^{+/+}$), heterozygous (*Gnrhr*$^{Ctail/+}$), and Ctail mice (*Gnrhr*$^{Ctail/Ctail}$) mice born from crosses of heterozygous mice. Pups were counted and genotyped at postnatal day 21. (D) WT and Ctail transcripts amplified from cDNA reverse transcribed from pituitary RNA of either WT (*Gnrhr*$^{+/+}$) or heterozygous (*Gnrhr*$^{Ctail/+}$) male mice with the recombined allele (after Cre-mediated recombination). PCR was performed using primers that amplify within exon 3 of the *Gnrhr*$^{+}$ transcript (primers Exon 3), or primers that amplify part of exon 3 and the Ctail (primers Exon3-Ctail). Minus RT (-RT) controls lack the reverse transcriptase enzyme.

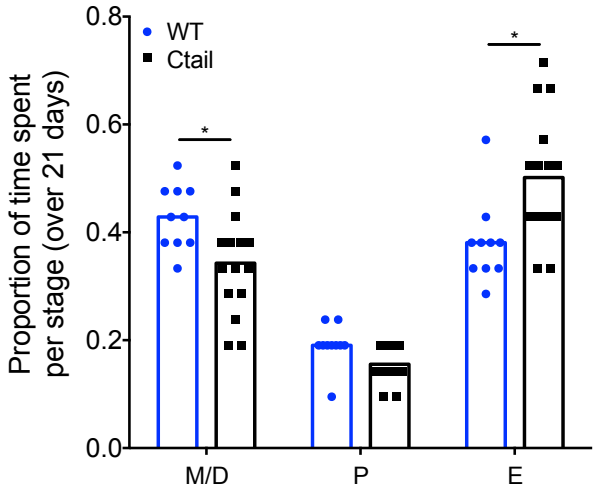

Figure 1-figure supplement 2: Ctail females exhibit altered estrous cyclicity. Proportion of time spent in each stage of the estrous cycle in WT and Ctail mice. Individual data points are shown as circles and squares. The height of the bars reflects the group means. Data at each cycle stage were analyzed with paired *t*-tests. Bars with different letters differed significantly. M/D, metestrus/diestrus (* p = 0.0099); P, proestrus (p = 0.2841); E, estrus (* p = 0.0003).

Figure 1-figure supplement 2

A

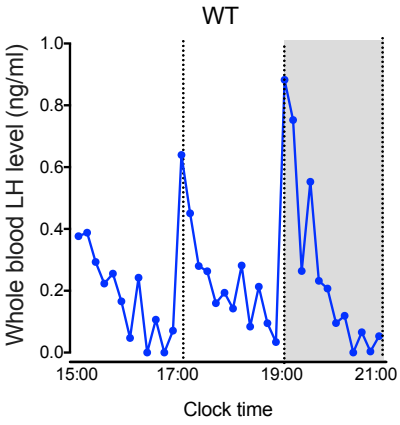

B

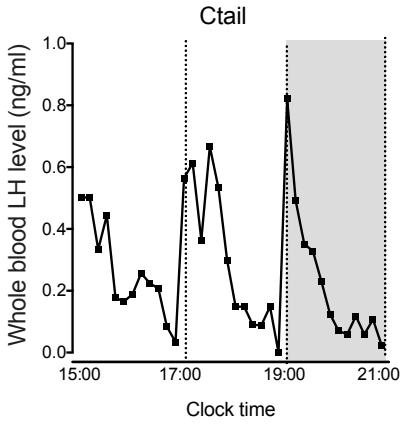

C

Deconvolution of 6-hour LH profiles

Genotype	WT (N=6)		Ctail (N=6)		
Parameter	Median	Range	Median	Range	P value
Pulse frequency (#/6h)	4	(2-7)	3	(2-7)	0.37
Slow half-life (min)	5.09	(4-11.55)	4	(4-12)	1
Mode (min)	13.3	(11.7-14.5)	16.9	(15.0-21.8)	0.003
Basal secretion (ng/mL/6h)	4.58	(0.36-31.5)	5.55	(1.06-37.5)	0.64
Pulsatile secretion (ng/mL/6h)	6.47	(1.20-23.8)	14.69	(0.97-23.7)	0.26
Total secretion (ng/mL/6h)	10.96	(1.65-45.0)	17.37	(2.03-61.0)	0.42
Mean pulse mass (ng/mL)	2.25	(0.38-3.96)	3.82	(0.48-7.35)	0.076
Weibull lambda (#/24h)	19.4	(11.9-26.8)	13.3	13.3(11.0-25.9)	0.27
AUC (ng. 6h/mL)	80	(4.8-163)	93	(6.4-22.8)	0.41
Jack ApEn (dimensionless)	1.211	(0.472-1.498)	1.198	(0.261-1.536)	0.67

Figure 2-figure supplement 1: Normal LH pulse frequency in male Ctail mice. Representative profiles of LH secretion from male (A) WT (blue) and (B) Ctail mice (black). Gray area represents the dark period of a 7AM/7PM light/dark cycle. Mice were sampled every 10 min over 6 hours. (C) Deconvolution analysis of LH release profiles over 6 hours from WT and Ctail mice (N = 6 per genotype). Student *t*-tests were performed for statistical analysis. Whole blood LH levels were measured using an in-house LH ELISA.

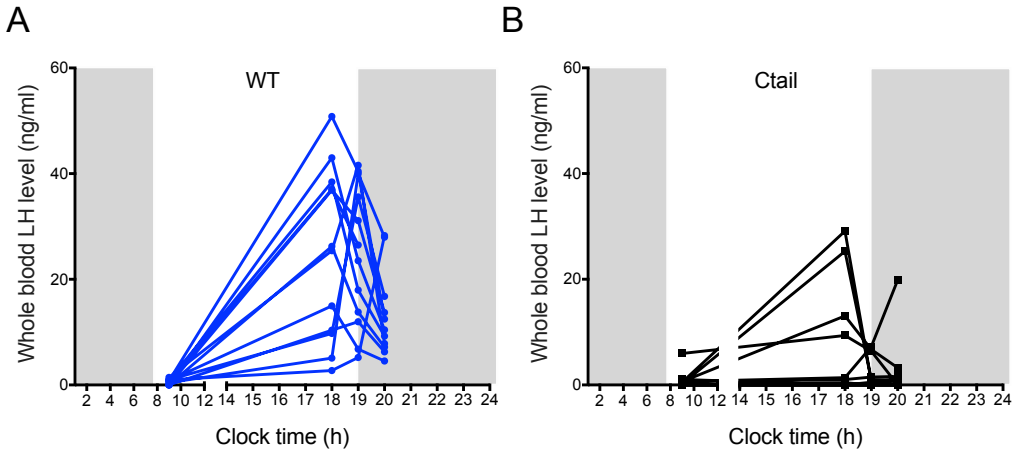

Figure 4-figure supplement 1: Ctail females exhibit altered LH surges. Whole blood LH levels measured at four different time points (10 am, and 6, 7, and 8 pm) on proestrus in (A) WT and (B) Ctail females. Each line reflects an individual mouse and data are only shown from mice that surged. The peak LH values from this analysis were used in Figure 4C.

Figure 4-figure supplement 1

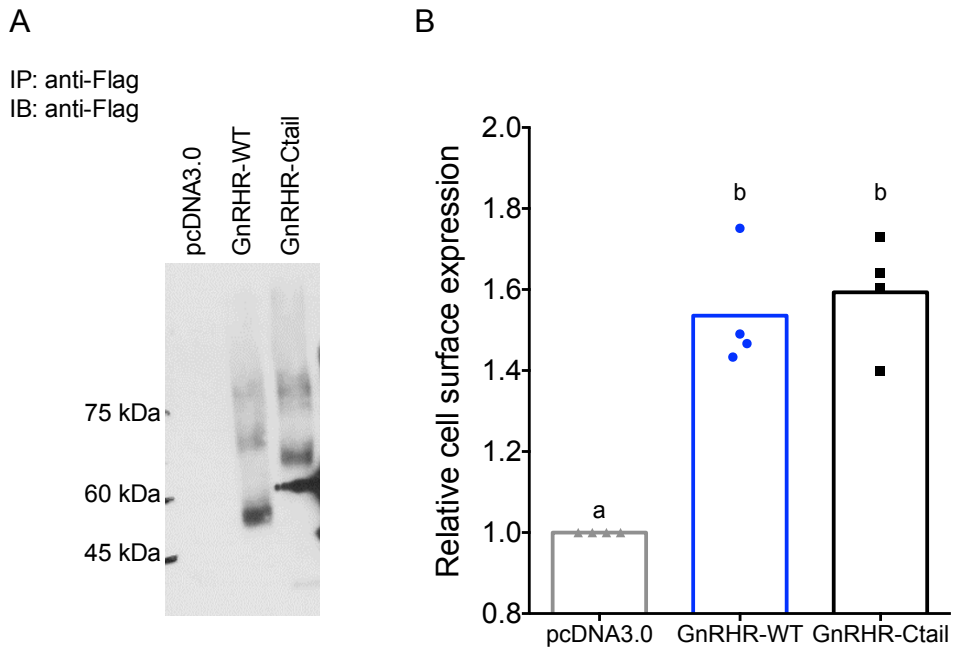

Figure 6-figure supplement 1: Cell surface expression of WT and Ctail receptors is comparable in HEK 293T cells. (A) HEK 293T cells were transfected with either flag-tagged GnRHR-WT or GnRHR-Ctail expression vector, or empty vector (pcDNA3.0) as control. Cell lysates were collected and immunoprecipitated (IP) using anti-Flag beads. Precipitates were than subjected to immunoblot (IB) using an anti-Flag antibody. The blot is from an individual experiment. (B) Whole cell anti-Flag ELISA performed on non-permeabilized HEK 293T cells expressing either GnRHR-WT or GnRHR-Ctail. pcDNA3.0 was used as a negative control. Cell surface receptor expression was quantified by dividing the OD450 for each receptor by the OD450 for pcDNA3.0. Data are shown from 4 independent experiments, with the bar height reflecting the group mean. Statistical analysis was performed using one-way ANOVA, followed by Tukey's post-hoc comparison. Bars with different letters differed significantly. pcDNA3.0 vs. GnRHR-WT $p = 0.0020$; pcDNA3.0 vs. GnRHR-Ctail $p = 0.0013$; GnRHR-WT vs. GnRHR-Ctail $p = 0.9495$.

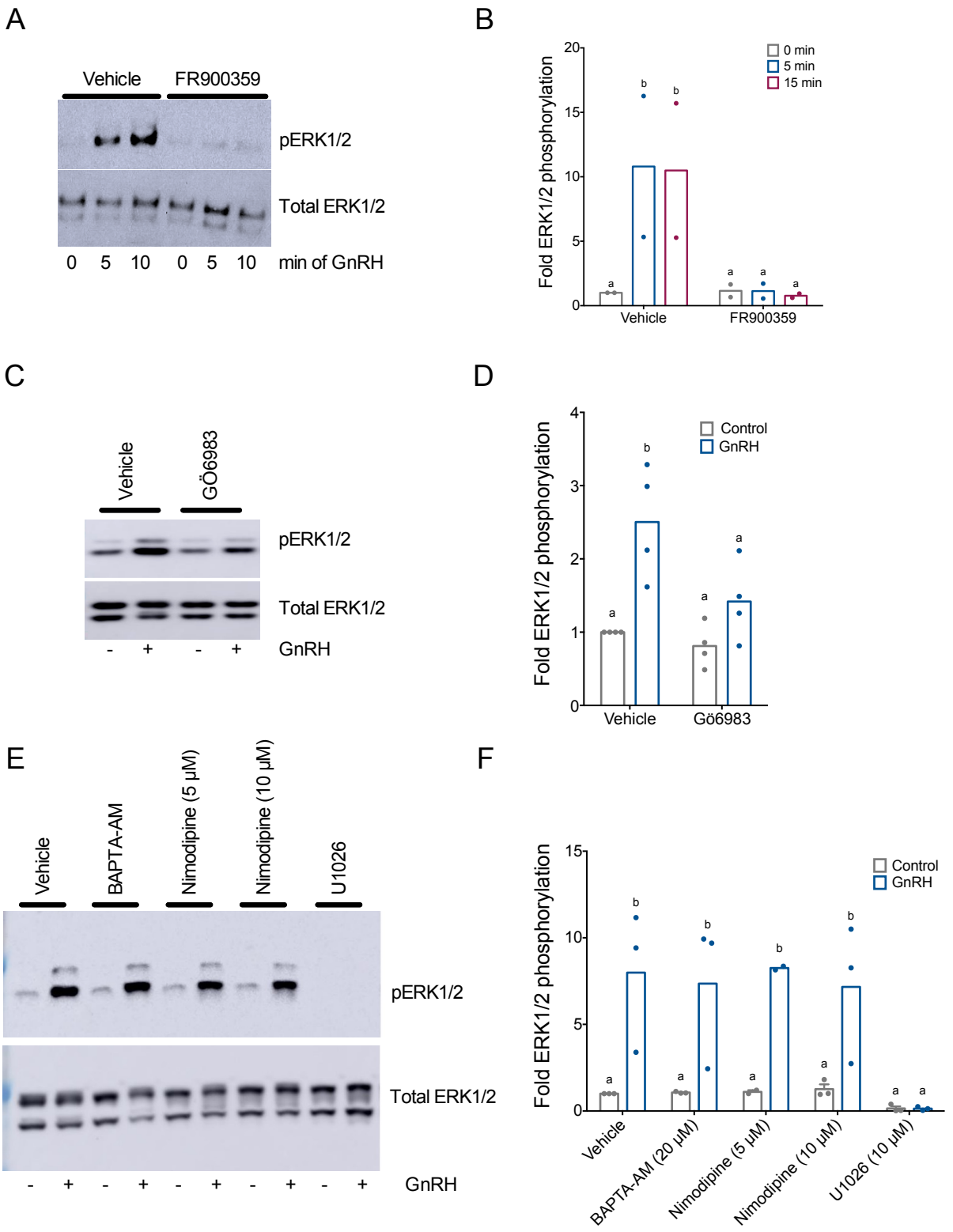

Figure 7-figure supplement 1

Figure 7-figure supplement 1: GnRH induced ERK1/2 phosphorylation is $G\alpha_{q/11}$- and PKC-dependent, and calcium-independent in homologous LβT2 cells. (A) LβT2 cells were pretreated with 10 μM FR900359 ($G\alpha_{q/11}$ inhibitor) or vehicle (DMSO) for 1 h, and then treated with vehicle (water) or 10 nM GnRH for 5- or 15-min. Whole cell protein lysates were collected and subjected to SDS-PAGE and western blotting with phospho- (top) or total (bottom) ERK1/2 antibodies. Blots from one of two replicate experiments are shown. (B) Data from independent duplicate experiments exemplified in panel A were quantified by normalizing the densitometry for the pERK1/2 bands to the total ERK1/2 bands. Data are presented as fold phospho-ERK1/2 relative to the control condition. Bar height reflects the group mean. Data were analyzed by two-way ANOVA, followed by Sidak's post-hoc comparison tests. Bars with different letters differed significantly. Vehicle vs. FR900359: 0 min GnRH $p > 0.9999$; 5 min GnRH $p = 0.0106$; 15 min GnRH $p = 0.0085$]. (C) LβT2 cells were pretreated for 20 min with vehicle (DMSO) or 5 μM Gö6983 for 20 min followed by treatment with vehicle (water) or 10 nM GnRH for 5 min. Western blots were performed as in panel A. (D) Data from 3 independent experiments in exemplified panel C were presented and quantified as in panel B. Data were analyzed by two-way ANOVA, followed by Sidak's post-hoc comparison tests. Bars with different letters differed significantly. Control (vehicle) vs. GnRH (vehicle) $p = 0.0048$; Control (Gö6983) vs. GnRH (Gö6983) $p = 0.3470$. Control (vehicle) vs. Control (Gö6983) $p = 0.9472$; GnRH (vehicle) vs. GnRH (Gö6983) $p = 0.0389$. (E) LβT2 cells were pretreated for 20 min with vehicle (DMSO), 20 μM BAPTA-AM, 5 μM or 10 μM nimodipine, or 10 μM U0126 for 20 min followed by vehicle (water) or 10 nM GnRH for 5 min. Western blots were performed as in panel A. (F) Data from 3 independent experiments in panel E were presented and quantified as in panel B. Data were analyzed by two-way ANOVA, followed by Sidak's post-hoc comparison tests. Bars with different letters differed significantly. Control vs. GnRH: Vehicle $p = 0.0103$; BAPTA-AM $p = 0.0229$; Nimodipine (5 μM) $p = 0.0377$; Nimodipine (10 μM) $p = 0.0350$; U1026 $p > 0.9999$.

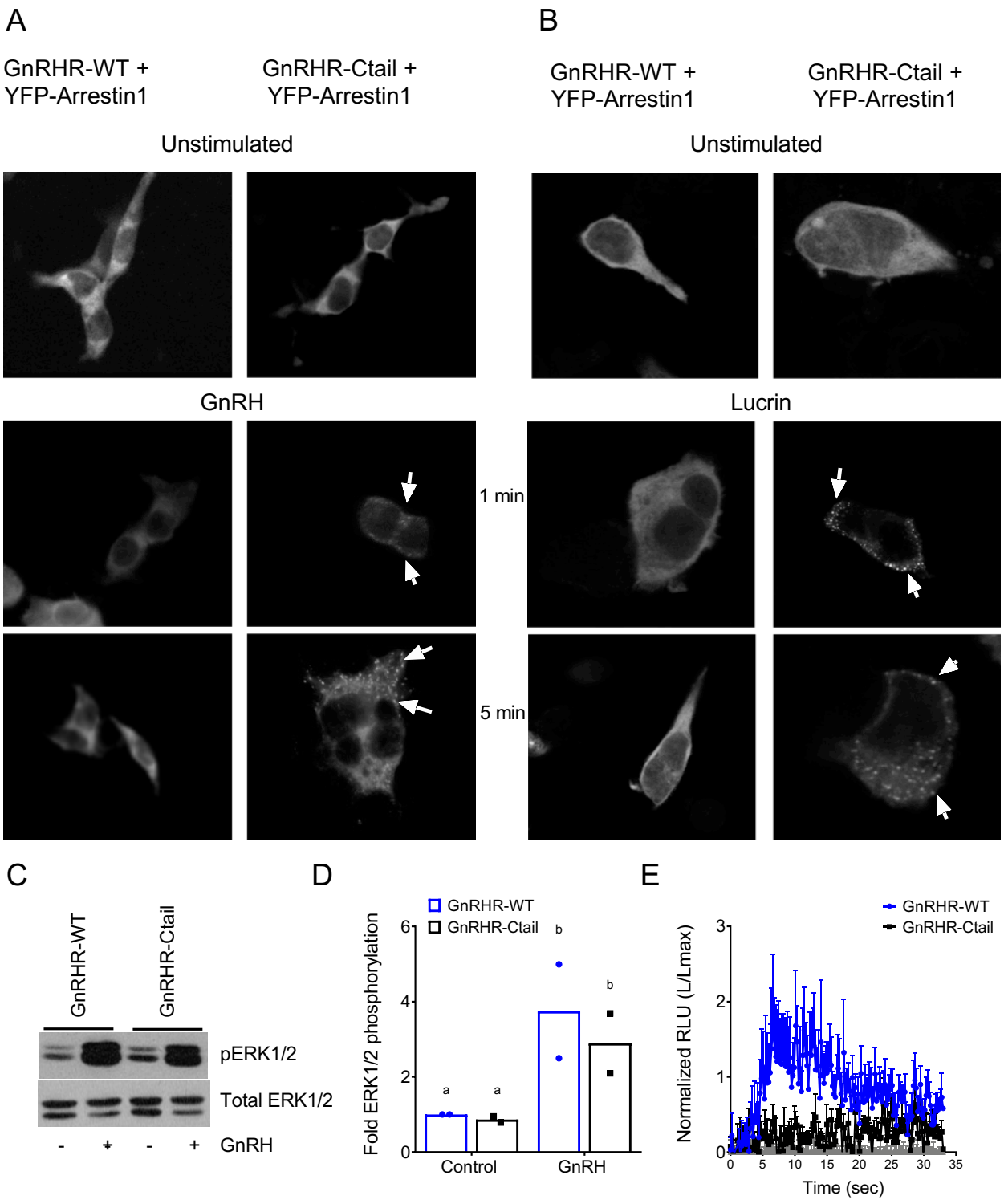

Figure 7-figure supplement 2

Figure 7-figure supplement 2: GnRH-induced pERK1/2 and calcium mobilization via GnRHR-Ctail are β-arrestin-independent. (A-B) HEK 293 cells were transfected with expression vectors for GnRHR-WT or GnRHR-Ctail along with YFP-β-arrestin-1. Cells were either left unstimulated or were treated with (A) 100 nM GnRH or (B) 1 μM Lucrin for 1 or 5 min. Cells were then fixed and imaged on a fluorescence microscope. Puncta at the cell membrane (white arrows) indicate the recruitment of β-arrestin-1. (C) β-arrestin-1/2 knockout (*Arr1*;*Arr2* KO) HEK 293T cells were transfected with GnRH-WT or GnRH-Ctail and treated with vehicle (water) or 100 nM GnRH for 5 min. Whole cell lysates were collected and subjected to western blotting for pERK1/2 and total ERK1/2 as in Figure 7-figure supplement 1. (D) Data from 2 independent experiments exemplified in panel C were quantified and analyzed as in Figure 7-figure supplement 1. Data are presented as fold phospho-ERK1/2 relative to the control condition. Data were analyzed by two-way ANOVA, followed by Sidak's post-hoc comparison tests. Bars with different letters differed significantly. GnRHR-WT (control) vs. GnRHR-Ctail (control) $p = 0.9178$; GnRHR-WT (control) vs. GnRHR-WT (GnRH) $p = 0.0115$; GnRHR-Ctail (control) vs. GnRHR-Ctail (GnRH) $p = 0.0334$; GnRHR-WT (GnRH) vs. GnRHR-Ctail (GnRH): $p = 0.2502$. (E) β-arrestin-1/2 KO HEK 293 cells were co-transfected with pcDNA3.0 (gray), GnRHR-WT (blue), or GnRHR-Ctail (black) expression vector and the Obelin biosensor. Cells were then treated with 100 nM GnRH. Luminescence was measured for 30 s at 22 ms intervals. Data from 3 independent experiments (mean ± SEM) are represented as the ratio of total luminescence after ligand injection over maximal luminescence (not shown) following Triton X-100 injection.

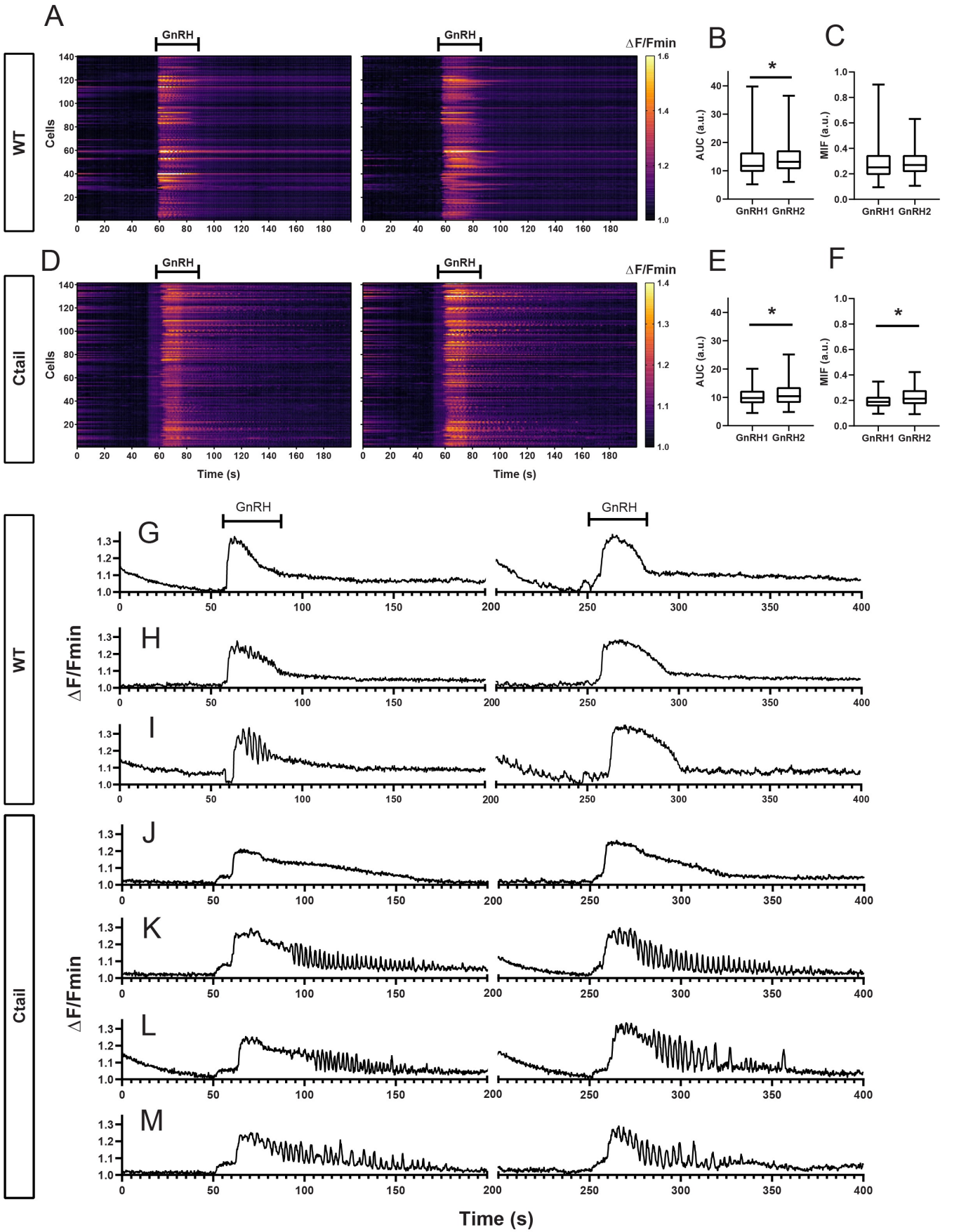

Figure 8-figure supplement 1

Figure 8-figure supplement 1: Gonadotropes of wild-type and Ctail mice respond to repeated GnRH pulses. Raster plots of calcium responses to first (left) and second (right) GnRH pulses in gonadotropes from a representative adult male (A) wild-type and (D) Ctail mouse. Each row represents an individual cell. Cells are numbered on the y-axis. The x-axis shows time in seconds. The timing of the two GnRH pulses is indicated. Pulses were separated by 60 min. The yellower colors reflect calcium responses. (B) Comparison of the AUC after each GnRH stimulus from one WT mouse (201 cells; 13.536 ± 6.093 vs. 14.241 ± 4.876 a.u. for GnRH1 and GnRH2, respectively; p = 0.0095). (C) Comparison of the MIF after each GnRH stimulus from one WT mouse (201 cells; 0.285 ± 0.138 vs. 0.281 ± 0.088 a.u. for GnRH1 and GnRH2, respectively; p = ns). (E) Comparison of the AUC after two GnRH pulses from one Ctail mouse (141 cells; 10.242 ± 3.151 vs. 11.173 ± 4.031 a.u. for GnRH1 and GnRH2, respectively; p = ns). (F) Comparison of the MIF after the two GnRH pulses from one Ctail mouse (141 cells; 0.196 ± 0.054 vs. 0.225 ± 0.076 a.u. for GnRH1 and GnRH2, respectively; p = 0.0020). Examples of calcium responses in individual gonadotropes from (G-I) wild-type and (J-M) Ctail mice. Statistical analyses were performed using Wilcoxon signed-rank tests.

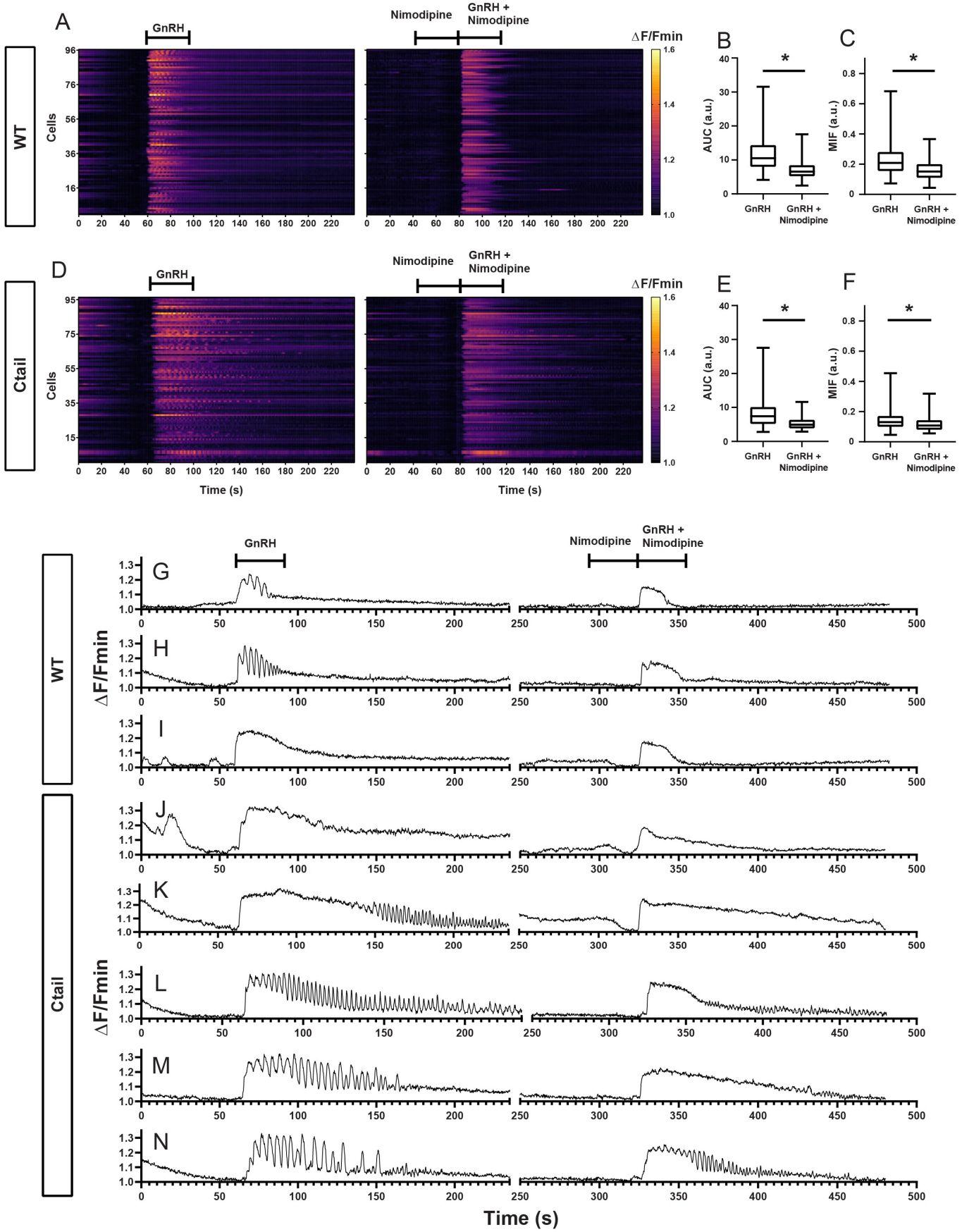

Figure 8-figure supplement 2

Figure 8-figure supplement 2: Nimodipine alters GnRH induced calcium responses in gonadotropes of wild-type and Ctail mice. The analysis in Figure 8-figure supplement 1 was repeated but with the L-type calcium channel blocker nimodipine (Nim) applied prior to and during the second GnRH pulse. Raster plots of GnRH induced calcium responses in the absence (left) and presence of nimodipine (right) in gonadotropes from a representative adult male (A) wild-type and (D) Ctail mouse. The two stimuli were separated by 60 min wash with Krebs-Ringer. Comparisons of AUC from a (B) wild-type (275 cells; 11.5 ± 4.7 vs. 7.1 ± 2.8 a.u. for GnRH and GnRH/Nim, respectively; $p < 0.0001$) and a (E) Ctail mouse (127 cells; 8.15 ± 3.9 vs. 5.4 ± 2.0 a.u. for GnRH and GnRH/Nim, respectively; $p < 0.0001$). Comparisons of MIF from the (C) wild-type (275 cells; 0.228 ± 0.101 vs. 0.163 ± 0.07 a.u. for GnRH and GnRH/Nim, respectively; $p < 0.0001$) and (F) Ctail mouse (127 cells; 0.145 ± 0.067 vs. 0.117 ± 0.046 a.u. for GnRH and GnRH/Nim, respectively; $p < 0.0001$). Examples of calcium responses in individual gonadotropes from (G-I) wild-type and (J-N) Ctail mice. Statistical analyses were performed using Wilcoxon signed-rank tests.

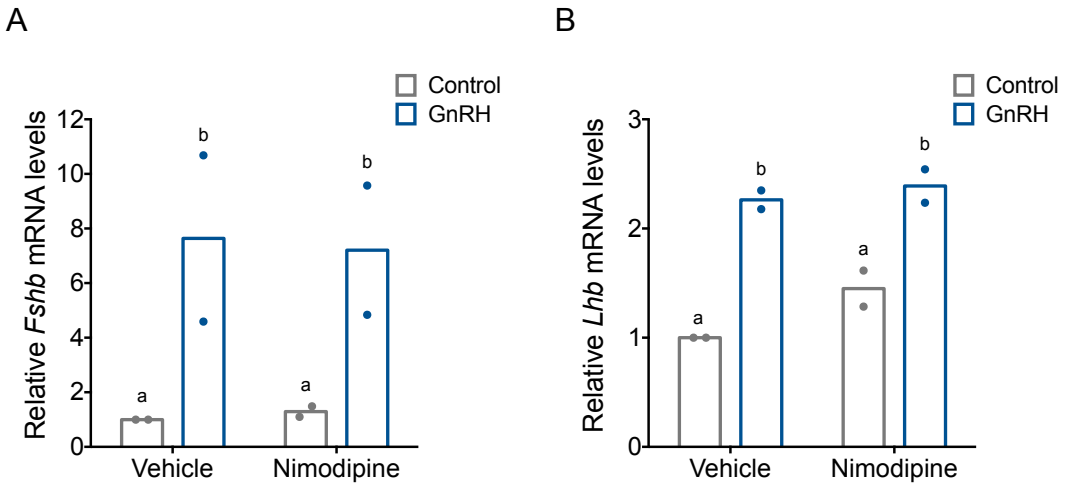

Figure 9-figure supplement 1: GnRH-induced *Fshb* and *Lhb* expression does not depend on calcium entry via L-type channels in homologous LβT2 cells. (A) Relative *Fshb* and (B) *Lhb* expression in LβT2 cells treated with vehicle (DMSO) or 10 μM nimodipine for 20 min followed by treatment with water (vehicle) or high frequency GnRH (10 nM) pulses. Gene expression was assessed by RT-qPCR and normalized to *Rpl19*. Data reflect the means of 2 independent experiments. Data were analyzed with two-way ANOVAs, followed by post-hoc Tukey's test for multiple comparisons. Bars with different letters differed significantly. Panel A: Control (vehicle) vs. GnRH (vehicle) $p = 0.0178$; Control (vehicle) vs. GnRH (Nimodipine) $p = 0.0232$; GnRH (vehicle) vs. GnRH (Nimodipine) $p = 0.8545$; Control (Nimodipine) vs. GnRH (Nimodipine) $p = 0.0235$. Panel B: Control (vehicle) vs. GnRH (vehicle) $p = 0.0061$; Control (vehicle) vs. GnRH (Nimodipine) $p = 0.0043$; GnRH (vehicle) vs. GnRH (Nimodipine) $p = 0.8770$; Control (Nimodipine) vs. GnRH (Nimodipine) $p = 0.0178$.

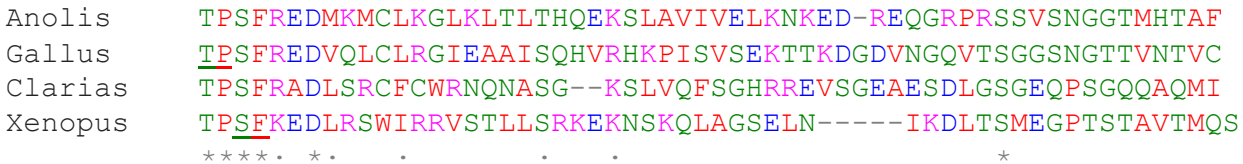

Figure 10-figure supplement 1: Alignment of the C-tails from the GnRHRs in chicken, frog, lizard, and catfish. The amino acid sequences of the GnRHR C-tails from *Gallus gallus* (NM_204653.1), *Xenopus laevis* (NM_001085707), *Anolis carolinensis* (XM_003226565.3) and *Clarias garepinus* (derived from closely related *Tachysaurus fulvidraco,* XM_027175679.1) were aligned using ClustalW. Different colors indicate different amino acid types: Red: small and hydrophobic; Blue: acidic; Magenta: basic; Green: hydroxyl, sulfhydryl, and amine. An asterisk (*) indicates conservation of the amino acid at that position. A colon (:) indicates similarity of amino acids at that position. Underlined amino acids were replaced by the *Cla*I restriction site in *Gallus* and *Xenopus* (translated to Ile-Asp) to clone the different C-tails downstream of the murine GnRHR. For *Clarias* and *Anolis*, the *Cla*I restriction site was added upstream of the sequences shown.

Figure 10-figure supplement 1